Variability of Absorption and Optical Properties of Key Aerosol Types Observed in Worldwide Locations

OLEG DUBOVIK,*,+ BRENT HOLBEN,* THOMAS F. ECK,*,# ALEXANDER SMIRNOV,*,+ YORAM J. KAUFMAN,@ MICHAEL D. KING,& DIDIER TANRÉ,** AND ILYA SLUTSKER*,+

*Laboratory for Terrestrial Physics, NASA Goddard Space Flight Center, Greenbelt, Maryland
+Science Systems and Applications, Inc., Lanham, Maryland
#Goddard Earth Sciences and Technology Center, University of Maryland Baltimore County, Baltimore, Maryland
@Laboratory for Atmospheres, NASA Goddard Space Flight Center, Greenbelt, Maryland
&Earth Science Directorate, NASA Goddard Space Flight Center, Greenbelt, Maryland
**Universite de Sciences et Techniques de Lille, Lille, France

(Manuscript received 21 December 2000, in final form 14 May 2001)

ABSTRACT

Aerosol radiative forcing is a critical, though variable and uncertain, component of the global climate. Yet climate models rely on sparse information of the aerosol optical properties. In situ measurements, though important in many respects, seldom provide measurements of the undisturbed aerosol in the entire atmospheric column. Here, 8 yr of worldwide distributed data from the AERONET network of ground-based radiometers were used to remotely sense the aerosol absorption and other optical properties in several key locations. Established procedures for maintaining and calibrating the global network of radiometers, cloud screening, and inversion techniques allow for a consistent retrieval of the optical properties of aerosol in locations with varying emission sources and conditions. The multiyear, multi-instrument observations show robust differentiation in both the magnitude and spectral dependence of the absorption—a property driving aerosol climate forcing, for desert dust, biomass burning, urban–industrial, and marine aerosols. Moreover, significant variability of the absorption for the same aerosol type appearing due to different meteorological and source characteristics as well as different emission characteristics are observed. It is expected that this aerosol characterization will help refine aerosol optical models and reduce uncertainties in satellite observations of the global aerosol and in modeling aerosol impacts on climate.

1. Introduction

The lack of detailed knowledge of the optical properties of aerosols results in aerosol being one of the largest uncertainties in climate forcing assessments (cf. Charlson et al. 1992; Houghton et al. 1996; Tegen et al. 1996; Hansen et al. 1997, 2000; Heintzenberg et al. 1997). Monitoring of atmospheric aerosol is a fundamentally difficult problem. First, compared to atmospheric gases, aerosol is highly inhomogeneous and variable; that is, aerosol observations have to be global and continuous. Second, the available accuracy of aerosol characterization is often not sufficient. For instance, in situ measurements traditionally considered as the most reliable observations are inappropriate for global monitoring of aerosol radiative forcing parameters and usually do not characterize the aerosol in the total atmospheric column (cf. Heintzenberg et al. 1997; Sokolik et al. 1993; Sokolik and Toon 1996). Satellite remote sensing provides nonintrusive measurements and global coverage; however, radiation measured from satellites depends on the earth's surface reflectance, and extraction of the aerosol contribution presently has a limited scope and accuracy (Kaufman et al. 1997a; King et al. 1999). Ground-based aerosol remote sensing does not provide global coverage; however, its wide angular and spectral measurements of solar and sky radiation are best suited to reliably and continuously derive the detailed aerosol optical properties in key locations. In spite of high temporal and spatial aerosol variability, there are a rather limited number of general categories of aerosol types with distinctly different optical properties. The following four general aerosol types are associated with different sources and emission mechanisms and are expected to exhibit significant differences in optical properties: (i) urban–industrial aerosol from fossil fuel combustion in populated industrial regions, (ii) biomass burning aerosol produced by forest and grassland fires, (iii) desert dust blown into the atmosphere by wind, and (iv) aerosol of marine origin. Detailed knowledge of the optical properties of these key aerosol types is needed to clarify the mechanisms of aerosol radiative forcing.

Corresponding author address: Oleg Dubovik, NASA Goddard Space Flight Center, Code 923, Greenbelt, MD 20771.
E-mail: dubovik@aeronet.gsfc.nasa.gov

Additionally, refining aerosol optical models is important for improving the accuracy of satellite retrieval algorithms that rely on assumptions of the optical properties associated with each aerosol type (e.g., King et al. 1999; Kaufman et al. 1997b; Tanré et al. 1997; Torres et al. 1998; Stowe et al. 1997; Kahn et al. 1998; Martonchik et al. 1998; etc.).

Modeling the aerosol effects on atmospheric radiation, by solving the radiative transfer equation, requires the following aerosol optical properties: aerosol optical thickness $\tau(\lambda)$ (loading); phase function $P(\Theta; \lambda)$ (angular dependence of light scattering), and single-scattering albedo $\omega_0(\lambda)$ (ratio of scattering to scattering + absorption). The sensitivity of radiative forcing to observed natural and anthropogenic variations of the above-listed optical properties characterizes the impact of the atmospheric aerosol on climate change. Studies (cf. Hansen et al. 1997) show that single-scattering albedo determines the sign (cooling/heating, depending on the planetary albedo) of the aerosol radiative forcing, while the asymmetry of the phase function together with optical thickness of the atmospheric aerosol drive the magnitude of the forcing. Most of the aerosol optical models (Shettle and Fenn 1979; WMO 1983; Koepke et al. 1997; Hess et al. 1998) associate aerosol radiative properties [$\tau(\lambda)$, $P(\Theta; \lambda)$, and $\omega_0(\lambda)$] with physical and chemical characteristics of the atmospheric aerosol: particle sizes, shape, and composition.

This strategy allows one to employ knowledge of the physics and chemistry of atmospheric aerosol for modeling aerosol optics and, vice versa, to infer some physical and chemical aerosol information from optical measurements (e.g., by remote sensing). However, an adequate modeling of the entire complexity of the interrelationship of optical, physical, and chemical aerosol properties is a fundamentally challenging task. On the other hand, the optical properties exhibit clear sensitivities to a rather limited set of physical and chemical features of the aerosol. Therefore, optical models (Shettle and Fenn 1979; WMO 1983; Koepke et al. 1997; Hess et al. 1998) employ the following confined set of the aerosol parameters: particle size (particle size distribution), composition (complex index of refraction), and shape (deviation from sphericity; e.g., Mischenko et al. 1997). Certainly, there are numerous studies suggesting sophistication of the optical model by various details, such as internal inhomogeneity of the particles, complex geometrical shapes of the particle, etc. Indeed, remarkable progress in modeling of light scattering by nonspherical particles achieved during the last two decades (e.g., Mishchenko et al. 2000) has significantly stimulated recognition of the issue of aerosol particle nonsphericity by the aerosol community and in many applications. Correspondingly, in both aerosol modeling and applications there are many efforts to account for particle nonsphericity (cf. Kahn et al. 1997; Krotkov et al. 1999, etc.), in particular by substituting the common assumption of spherical aerosol by randomly oriented spheroids (Mishchenko et al. 1997). Nevertheless, nonsphericity as well as inhomogeneity are not completely clarified issues in atmospheric aerosol modeling and most aerosol applications rely on an optical model that considers aerosol as a mixture of spherical homogeneous particles of different sizes with composition characterized by the complex refractive index. Scientific experience indicates that, in many cases, these assumptions allow models to adequately reproduce the observed aerosol affected radiation fields.

Obviously, wide acceptance of optical models based on the above-described simplified assumptions reflects the limitations of present aerosol knowledge and does not mean that in reality the aerosol exists as an ensemble of chemically homogeneous particles of regular shape. Clarifying the details of physical and chemical aerosol structure and their connections with optical properties requires the involvement of physical and chemical aerosol analysis, which are provided by many kinds of in situ aerosol measurements. Correspondingly, in the present paper, we will verify and enrich the aerosol properties derived from ground-based remote sensing of aerosol by intercomparisons with available in situ aerosol information.

Present aerosol radiation models are particularly uncertain concerning values of the single-scattering albedo $\omega_0(\lambda)$ (Kaufman et al. 1997a). The magnitude of $\omega_0(\lambda)$ is mostly dependent on the complex part of the refractive index $k(\lambda)$ and particle size. For example, $\omega_0(\lambda)$ of desert dust simulated according to a number of models (Shettle and Fenn 1979; WMO 1983; Koepke et al. 1997; Hess et al. 1998) ranges from 0.63 to 0.87 at 0.5 μm, while aircraft radiation measurements (Fouquart et al. 1987a) suggest lower absorption ($\omega_0 = 0.95$ for the broadband solar spectrum). Such uncertainty is unacceptable, since even smaller changes of ω_0 (from 0.95 to 0.85) would change the radiative forcing of desert dust from significant cooling to significant warming (Hansen et al. 1997). In addition, even a low loading of the absorbing aerosol [$\omega_0(550) \sim 0.88$)] may affect radiative forcing semidirectly by evaporating clouds (Ackerman et al. 2000). The optical properties of pure black carbon (soot)—a component of smoke and urban–industrial aerosol driving aerosol absorption—has been widely studied. However, aerosol absorption depends also on the mixing mechanism of soot with other aerosol components (Ackerman and Toon 1981; Martins et al. 1998; Jacobson 2001). This, in addition to measurement uncertainties, is why the ω_0 reported in the literature (Shettle and Fenn 1979; WMO 1983; Remer et al. 1998; Reid et al. 1998) for absorbing aerosol ranges from nearly 1.0 to 0.6 with unclear spectral dependence. The optical properties of the urban component are reported in a number of models (Shettle and Fenn 1979; WMO 1983; Koepke et al. 1997; Hess et al. 1998); however, the presence and relative contribution of this component in the total column of the ambient aerosol is rather uncertain. Models of urban–industrial columnar aerosol

are sometimes based on single locality studies (Remer and Kaufman 1998) and the possible discrimination of the urban aerosol by concentration level and type of local pollution is unclear.

Thus, taking into account both the lack of the reliable information on aerosol absorption (Kaufman et al. 1997a) and, its critical importance for aerosol radiative forcing assessments (Hansen et al. 1997, 2000), we will focus the present analysis on a discussion of the observed aerosol absorption. We discuss the single scattering albedo as a parameter characterizing absorption, because radiative transfer properties are sensitive to absorption via sensitivity to the ratio of scattering to total extinction (scattering + absorption) rather than the absolute value of absorption. Therefore, the spectral dependence of ω_0 is driven by the spectral dependence of both absorption and scattering (e.g., Dubovik et al. 1998).

2. Observations and methodology

The Aerosol Robotic Network (AERONET; Holben et al. 1998) of ~100 identical globally distributed sun- and sky-scanning ground-based automated radiometers provides measurements of aerosol optical properties, based on up to 8 yr of observations in some locations. These data have the potential to narrow the uncertainty in knowledge of the aerosol optical properties. The spectral sky radiance is measured in a wide angular range from the sun and is minimally affected by surface reflectance (cf. Dubovik et al. 2000). The standardized network procedures (Holben et al. 1998; Smirnov et al. 2000b) of instrument maintenance, calibration, cloud screening, and data processing allow for quantitative comparison of the aerosol data obtained in different times and locations. The new AERONET inversion algorithm (Dubovik and King 2000) provides improved aerosol retrievals by fitting the entire measured field of radiances—sun radiance and the angular distribution of sky radiances—at four wavelengths (0.44, 0.67, 0.87, and 1.02 μm) to a radiative transfer model. The radiation field is driven by the (wavelength dependent) aerosol complex index of refraction and the particle size distribution (in the size range: $0.05 \leq r \leq 15$ μm) in the total atmospheric column. Using such a general aerosol model in the retrieval algorithm allows us to derive the aerosol properties with minimal assumptions. Only spectral and size smoothness constraints are used, preventing unrealistic oscillations in either parameter (Dubovik and King 2000).

a. Accuracy assessment of individual retrievals

The accuracy of individual retrievals was analyzed by extensive sensitivity simulations (Dubovik et al. 2000), studying the effects of both random measurement errors and systematic instrumental offsets for several aerosol models. The analysis showed that an accurate $\omega_0(\lambda)$ retrieval (with accuracy to the level of 0.03) and complex index of refraction (errors on the order of 30%–50% for the imaginary part of the refractive index and 0.04 for the real part of the refractive index) can be retrieved only for high aerosol loading [$\tau_{aer}(440) \geq 0.5$] for solar zenith angle $>50°$ (i.e., the range of scattering angles in measured solar almucantar $>100°$). For observations with lower aerosol loading, the retrieval accuracy of $\omega_0(\lambda)$, $k(\lambda)$, and $n(\lambda)$ significantly decreases because of a decrease of the information content. Indeed, the calibration accuracy becomes an obstacle because it causes an error in measuring τ_{aer} ($\Delta\tau_{aer} = \pm 0.01$) that is on the order of at least of 5%–10% of the optical thickness for $\tau_{aer}(440) \leq 0.2$, and it is comparable with the absorption partition in the total optical thickness. Correspondingly, the retrieval of $\omega_0(\lambda)$ and $k(\lambda)$ becomes difficult, as well as $n(\lambda)$, because scattering effects of $n(\lambda)$ and $k(\lambda)$ are not completely independent. Thus, our studies (Dubovik et al. 2000) have shown that for $\tau_{aer}(440) \leq 0.2$, the accuracy levels drop down to 0.05–0.07 for $\omega_0(\lambda)$, to 80%–100% for the imaginary part of the refractive index, and to 0.05 for the real part of the refractive index.

The retrieval of the particle volume size distribution was demonstrated to be adequate in practically all situations [e.g., $\tau_{aer}(440) \geq 0.05$], as demonstrated by Dubovik et al. (2000). These studies show that the error of the retrieved volume density $dV(r)/d\ \ln r$ changes as a nonlinear function of particle size, aerosol type, and actual values of the size distribution. In particular, for the intermediate particle size range ($0.1 \leq r \leq 7$ μm), the retrieval errors do not exceed 10% in the maxima of the size distribution and may increase up to about 35% for the points corresponding to the minimum values of $dV(r)/d\ \ln r$ in this size range. For the edges ($0.05 \leq r < 0.1$ μm, and $7 < r \leq 15$ μm) of the assumed particle size interval, the accuracy of the size distribution retrieval drops significantly, because of the low sensitivity of the aerosol scattering at 0.44, 0.67, 0.87, and 1.02 μm to particles of these sizes. Correspondingly, the retrieval errors rise up to 80%–100% (and even higher) for the sizes less than 0.1 μm and higher than 7 μm. The high errors at the edges do not significantly affect the derivation of the main features of the particle size distribution (concentration, median and effective radii, etc.), because typically the aerosol particle size distributions [$dV(r)/d\ \ln r$] have low values at the edges of retrieval size interval.

The aerosol particles in the retrieval are assumed to be polydispersed homogeneous spheres. Dubovik et al. (2000) showed how such assumptions bias the retrievals in the case of nonspherical aerosols or externally/internally mixed spheres. The tests showed that for externally/internally mixed spheres the assumption of spheres with effective refractive index is sufficient for reproducing AERONET observations and retrieval of the main radiative properties of the aerosol (absorption and scattering). Light scattering by nonspherical parti-

cles can be clearly detected in the retrieval, which assumes spheres, and these retrieval results need to be corrected. Namely, artificially high concentrations of very small particles with radii less than 0.1 μm can be obtained if the inversion uses observations at solar zenith angles of 20° or higher (scattering angles of ≥40°). This artifact disappears if the fine mode of particle size distributions was adopted from retrievals relying on measurements at scattering angles less than 40°. Also, nonspherical scattering causes an artificial spectral dependence of the real part of the refractive index and only values obtained for long wavelengths (870 and 1020 nm) are close to the true values. Nevertheless, our tests have shown that $\omega_0(\lambda)$ and $k(\lambda)$ [and $n(\lambda)$ at 0.87 and 1.02 μm] of nonspherical dust particles can be retrieved using an assumption of sphericity nearly as accurately as for truly spherical aerosol for high aerosol loading [$\tau_{aer}(440) \geq 0.5$] in addition to solar zenith angle >50°.

Also, we have shown (Dubovik et al. 2000) that the minimum value of the residual given by the best fit of measured radiances to a theoretical model is sensitive to both the presence of experimental error and the failure of the radiative model. The fitting error in absence of strong systematic biases is usually less than 5% (maximum 7%). Therefore, this residual value can be adopted as an indicator of the quality of the retrieval.

The accuracy levels described above are expected for AERONET retrieval in cloud-free conditions. The sky radiance measured in the solar almucantar is checked for symmetry. Indeed, for a spatially homogeneous atmosphere the sky radiances in the left and right parts of the measured almucatar should be very similar. Correspondingly, any local asymmetry of the left and right parts of the almucantar is an indication of cloud or other inhomogeneity and this measurement (scattering angle) can be eliminated from the inversion. Correspondingly, for a partially cloudy or perturbed atmosphere, the inverted almucantars have a strongly reduced number of scattering angles per almucantar. We consider these data as less reliable and do not include them in our analysis if the criterion of the symmetry was satisfied at less than 21 scattering angles (from a maximum of 26) in the measured almucantar.

b. Quality control criteria for individual retrieval

Thus, in order to use the retrieved aerosol information of the highest accuracy in our analysis, we selected the data according to the following criteria.

1) Only symmetrical almucantars were used for retrievals (symmetry criterion was satisfied at ≥21 scattering angles).
2) The results were used only from the retrievals with fitting accuracy of 5% or less (this was not applied to dust retrievals, where fitting error increases to ~15% due to nonspherical scattering).
3) The retrieved values of $\omega_0(\lambda)$, $k(\lambda)$, and $n(\lambda)$ [for dust $n(\lambda)$ only at 0.87 and 1.02 μm] were utilized only from the retrieval obtained for high aerosol loading $\tau_{aer}(440) \geq 0.5$ (except marine aerosol for which typical loading is much lower) and for solar zenith angle ≥50°.
4) For dust, the shape of the size distribution for fine particles ($r < 0.6$ μm) was adopted only from the retrievals obtained from sky-radiance measurements in the scattering angular range 40° or less.

c. Retrieval data presentation

We focused our analysis on 12 selected aerosol sites with well-known meteorological and environmental conditions where all four principal aerosol types can be identified. We included a mixed aerosol over the Maldives, which was extensively analyzed during the INDOEX closure experiment (Ramanathan et al. 2001, hereafter R01; Satheesh et al. 1999). Preference was given to data obtained at a given site by several instruments and/or during long periods of time (multiyear data were prioritized). Figure 1 and Table 1 summarize our analysis. The figure highlights the aerosol spectral single-scattering albedo. Figure 1 shows urban–industrial, biomass burning, desert dust and mixed aerosol interpolated for heavy loading conditions $\tau_{ext}(440) = 0.7$. As an exception, we used $\tau_{ext}(440) = 0.15$ for oceanic aerosol, because the loading does not reach a higher value for maritime aerosol. Table 1 covers the complete range of τ_{ext} observed for each aerosol type and shows the complex refractive index and the parameters of the biomodal volume particle size distribution. Namely, for each mode of the volume particle size distribution [$dV(r)/d\ \ln r$] we compute the particle volume concentration, the median radius, and the standard deviation (formulas given in the appendix). For this analysis, we defined all particles with radius smaller than 0.6 μm as belonging to the fine mode and all particles with radius larger than 0.6 μm as belonging to the coarse mode. In fact, practically all observed size distributions have bimodal structure with quite wide local minimum with low values of $dV(r)/d\ \ln r$ around 0.6 μm. The exact location of the inflection point is not critical for estimating C_{Vi}, r_{Vi}, and σ_i.

Many studies indicate that a bimodal lognormal function is the most appropriate model for aerosol particle size distributions (cf. Whitby 1978; Shettle and Fenn 1979; Remer and Kaufman 1998; etc.):

$$\frac{dV(r)}{d\ \ln r} = \sum_{i=1}^{2} \frac{C_{V,i}}{\sqrt{2\pi}\sigma_i} \exp\left[-\frac{(\ln r - \ln r_{V,i})^2}{2\sigma_i^2}\right], \quad (1)$$

where C_{Vi} denotes the particle volume concentration, r_{Vi} is the median radius, and σ_i is the standard deviation. Indeed, the retrieved average size distributions shown in Fig. 1 exhibit a distinct bimodality with shapes visually close to lognormal curves. Some deviations of

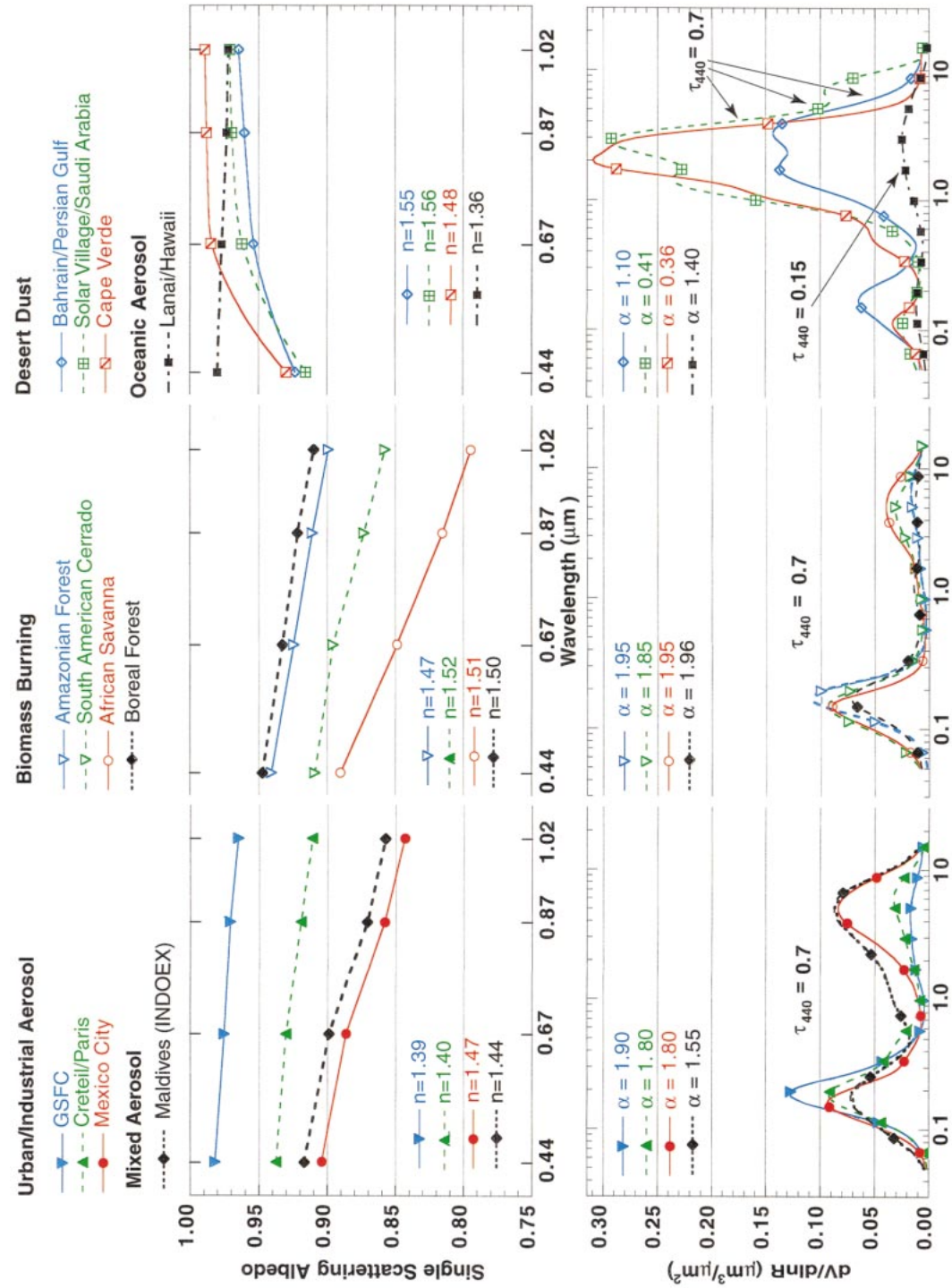

FIG. 1. The averaged optical properties of different types of tropospheric aerosol retrieved from the worldwide AERONET network of ground-based radiometers. Urban–industrial, biomass burning, and desert dust aerosols are shown for $\tau_{ext}(440) = 0.7$. Oceanic aerosol is shown for $\tau_{ext}(440) = 0.15$ since oceanic background aerosol loading does not often exceed 0.15. Also, $\omega_0(\lambda)$ and the refractive index n shown for Bahrain was obtained only for the cases when $\alpha \leq 0.6$ [for higher α, $\omega_0(\lambda)$ and refractive index n were very variable due to a significant presence of urban–industrial aerosol]. However, we show the particle size distribution representing all observations in Bahrain (complete range of α). Ångström parameter α is estimated using optical thickness at two wavelengths: 440 and 870 nm.

each mode from true lognormality, such as asymmetry, appearance of local peaks, etc. are present but they are unlikely to have a significant radiative effect. It should be noted that our equations (see appendix) for computing C_{Vi}, r_{Vi}, and σ_i are simple, general, and their formulation does not assume any function for the size distribution. Nevertheless, we formulated these equations so that they give the parameters of a lognormal size distribution if a true lognormal size distribution is observed. Correspondingly, the simplest and, according to our tests, quite accurate way of simulating aerosol optical properties with the parameters given in Table 1 is using a lognormal function.

We represented aerosol concentration (and other parameters with dynamic variability) as a function of optical thickness in a manner similar to other dynamic aerosol models (Remer and Kaufman 1998; Remer et al. 1998), which can help with the parameterization of aerosols in climate models and satellite remote sensing. Presenting aerosol optical properties as regressions with optical thickness helps to outline the dynamics of the aerosol optical properties associated with the growth of the aerosol mass and aerosol processes (aging, particle size and composition transformations, etc.) stimulated by the accumulation of aerosol in the atmosphere. Additionally, we present the Ångström parameter (Ångström 1929) α, defined by the spectral dependence of the optical thickness $\tau(\lambda) \sim \lambda^{-\alpha}$ and computed from two wavelengths, 440 and 870 nm. Here, α is a basic measure of the aerosol size distribution: $\alpha \sim 0$ corresponds to large dust particles, $\alpha \sim 2$ corresponds to small smoke particles. The single-scattering albedo is a function of the refractive index (mainly its imaginary part) and particle size. Therefore, we try to identify how specific features in $\omega_0(\lambda)$ are related to features in $dV(r)/d\ \ln r$ and $k(\lambda)$ and suggest a cause (physical, geographical, meteorological, etc.) responsible for each feature.

d. Data limitations

The limitations of the presented data set should be outlined.

First, sky-radiance measurements in general introduce sampling bias, because cloudy days are underrepresented in the database (cf. Remer et al. 1997).

The inversion stability criteria [such as high aerosol loading required for more accurate retrieval of $n(\lambda)$, $k(\lambda)$, and $\omega_0(\lambda)$] introduce additional biases. Nevertheless, these biases hardly decrease the value of the retrieval results, because many other measurement techniques would likely suffer from somewhat similar difficulties under low aerosol loading conditions. Indeed, low aerosol concentrations produces radiance fields of rather small magnitude, which can easily be corrupted or distorted during detection by minor natural or instrumental disturbances to the level where the effect of a property such as aerosol absorption is almost indistinguishable. Also, larger uncertainties in absorption (and index of refraction) at lower optical thickness likely would have less impact on radiative forcing assessments and remote sensing developments. However, we do not wish to imply that aerosol absorption is not important at low optical depths below 0.5 (e.g., at 440 nm). For example, Ackerman et al. (2000) have shown that absorbing aerosol at $\tau_{ext}(550) = 0.2$ with $\omega_0(550) = 0.88$ can result in reduced cloud coverage as a result of solar heating from aerosol in the boundary layer.

We choose to represent the retrieved aerosol properties as regressions with optical thickness in the absence of discrimination of seasonal and meteorological variations in the optical properties. It should be noted that for some aerosol sites considered, high optical thickness (desirable for aerosol absorption retrieval) was observed only seasonally. We indicated such seasonality in Table 1 for sites where it was observed. More detailed information on the seasonal and meteorological variability of the aerosol properties for several of these sites can be found in the studies by Holben et al. (2001), Eck et al. (1998, 2001a,b) and Smirnov et al. (2000a, 2002a, b), etc.

The retrieved parameters $dV/d\ \ln r$, $n(\lambda)$, and $k(\lambda)$ are not independent in the sense that the retrieval technique insures only the fact that the retrieved combination of all of these parameters would accurately reproduce the measured radiation field in the scope of the chosen radiative transfer model. Correspondingly, the retrieval accuracy of each individual aerosol parameter $dV/d\ \ln r$, $n(\lambda)$, and $k(\lambda)$ is dependent on the accuracy of our radiative transfer model.

3. Aerosol optical property characterization

a. Biomass burning aerosol

1) 1) SINGLE-SCATTERING ALBEDO

Figure 1 compares $\omega_0(\lambda)$ for all the sites studied. Biomass burning smoke is known as an absorbing aerosol with high concentration of black carbon produced by combustion. However, our data show that the value of ω_0 varies significantly for smoke of different origin (and possibly age) and correlates with the presence of black carbon in the combustion products. The highest absorption (lowest ω_0) with the strongest spectral dependence was observed for African savanna regions. The lowest absorption was observed for the two forested regions with ω_0 values very similar to each other at all wavelengths, even though these regions are very dissimilar in forest type and structure (Amazonian tropical forest versus North American boreal forest). The ω_0 values of the South American cerrado region are intermediate in magnitude. Much of the differences in absorption magnitude between these regions may be attributed to differences in the relative percentage of combustion occurring in the flaming versus the smoldering phases. Extensive field measurements in both Brazil and Africa (Ward et al. 1992, 1996) have shown that for

TABLE 1. Summary of aerosol optical properties retrieved from worldwide AERONET network of ground-based radiometers.

Urban–industrial and mixed	GSFC, Greenbelt, MD (1993–2000)	Crete–Paris, France (1999)
Number of measurements (total)	2400	300
Number of measurements (for ω_0, n, k)	200 (Jun–Sep)	40 (Jun–Sep)
Range of optical thickness; $\langle\tau\rangle$	$0.1 \le \tau(440) \le 1.0$; $\langle\tau(440)\rangle = 0.24$	$0.1 \le \tau(440) \le 0.9$; $\langle\tau(440)\rangle = 0.26$
Range of Ångström parameter	$1.2 \le \alpha \le 2.5$	$1.2 \le \alpha \le 2.3$
$\langle g\rangle$ (440/670/870/1020)	0.68/0.59/0.54/0.53 ± 0.08	0.68/0.61/0.58/0.57 ± 0.07
n; k	$1.41 - 0.03\tau(440) \pm 0.01$; 0.003 ± 0.003	1.40 ± 0.03; 0.009 ± 0.004
ω_0(440/670/870/1020)	0.98/0.97/0.96/0.95 ± 0.02	0.94/0.93/0.92/0.91 ± 0.03
r_{Vf} (μm); σ_f	$0.12 + 0.11\,\tau(440) \pm 0.03$; 0.38 ± 0.01	$0.11 + 0.13\,\tau(440) \pm 0.03$; 0.43 ± 0.05
r_{Vc} (μm); σ_c	$3.03 + 0.49\,\tau(440) \pm 0.21$; 0.75 ± 0.03	$2.76 + 0.48\,\tau(440) \pm 0.30$; 0.79 ± 0.05
C_{Vf}($\mu m^3/\mu m^2$)	$0.15\,\tau(440) \pm 0.03$	$0.01 + 0.12\,\tau(440) \pm 0.04$
C_{Vc}($\mu m^3/\mu m^2$)	$0.01 + 0.04\,\tau(440) \pm 0.01$	$0.01 + 0.05\,\tau(440) \pm 0.02$
Biomass burning	**Amazonian forest, Brazil (1993–1994); Bolivia (1998–1999)**	**South American cerrado, Brazil (1993–1995)**
Number of measurements (total)	700	550
Number of measurements (for ω_0, n, k)	250 (Aug–Oct)	350 (Aug–Oct)
Range of optical thickness; $\langle\tau\rangle$	$0.1 \le \tau(440) \le 3.0$; $\langle\tau(440)\rangle = 0.74$	$0.1 \le \tau(440) \le 2.1$; $\langle\tau(440)\rangle = 0.80$
Range of Ångström parameter	$1.2 \le \alpha \le 2.1$	$1.2 \le \alpha \le 2.1$
$\langle g\rangle$ (440/670/870/1020)	0.69/0.58/0.51/0.48 ± 0.06	0.67/0.59/0.55/0.53 ± 0.03
n; k	1.47 ± 0.03; 0.00093 ± 0.003	1.52 ± 0.01; 0.015 ± 0.004
ω_0(440/670/870/1020)	0.94/0.93/0.91/0.90 ± 0.02	0.91/0.89/0.87/0.85 ± 0.03
r_{Vf} (μm); σ_f	$0.14 + 0.013\tau(440) \pm 0.01$; 0.40 ± 0.04	$0.14 + 0.01\tau(440) \pm 0.01$; 0.47 ± 0.03
r_{Vc} (μm); σ_c	$3.27 + 0.58\tau(440) \pm 0.45$; 0.79 ± 0.06	$3.27 + 0.51\tau(440) \pm 0.39$; 0.79 ± 0.04
C_{Vf} ($\mu m^3/\mu m^2$)	$0.12\,\tau(440) \pm 0.05$	$0.1\,\tau(440) \pm 0.06$
C_{Vc} ($\mu m^3/\mu m^2$)	$0.05\,\tau(440) \pm 0.02$	$0.04 + 0.03\,\tau(440) \pm 0.03$
Desert dust and oceanic	**Bahrain–Persian Gulf (1998–2000)**	**Solar-Vil.–Saudi Arabia (1998–2000)**
Number of measurements (total)	1800	1500
Number of measurements (for ω_0, n, k)	100	250
Range of optical thickness; $\langle\tau\rangle$	$0.1 \le \tau(1020) \le 1.2$, $\langle\tau(1020)\rangle = 0.22$	$0.1 \le \tau(1020) \le 1.5$; $\langle\tau(1020)\rangle = 0.17$
Range of Ångström parameter	$0 \le \alpha \le 1.6$	$0.1 \le \alpha \le 0.9$
$\langle g\rangle$ (440/670/870/1020)	0.68/0.66/0.66/0.66 ± 0.04	0.69/0.66/0.65/0.65 ± 0.04
n	1.55 ± 0.03	1.56 ± 0.03
k(440/670/870/1020)	0.0025/0.0014/0.001/0.001 ± 0.001	0.0029/0.0013/0.001/0.001 ± 0.001
ω_0(440/670/870/1020)	0.92/0.95/0.96/0.97 ± 0.03	0.92/0.96/0.97/0.97 ± 0.02
r_{Vf} (μm); σ_f	0.15 ± 0.04; 0.42 ± 0.04	0.12 ± 0.05; 0.40 ± 0.05
r_{Vc} (μm); σ_c	2.54 ± 0.04; 0.61 ± 0.02	2.32 ± 0.03; 0.60 ± 0.03
C_{Vf} ($\mu m^3/\mu m^2$)	$0.02 + 0.1\,\tau(1020) \pm 0.05$	$0.02 + 0.02\,\tau(1020) \pm 0.03$
C_{Vc} ($\mu m^3/\mu m^2$)	$-0.02 + 0.92\,\tau(1020) \pm 0.04$	$-0.02 + 0.98\,\tau(1020) \pm 0.04$

* Each value in the table is accompanied by a std dev, for example, ±0.01 (this is not an accuracy of the retrieval). The values of real and imaginary parts of the refractive index, as well as single-scattering albedo, are given only for the condition of $\tau(440) \ge 0.4$ for Urban–industrial, mixed, and biomass burning aerosols, and for the conditions of $\tau_{ext}(1020) \ge 0.3$ and $\alpha \le 0.6$ for desert dust. The parameters of particle size distribution are given for complete observed ranges in optical thickness and Ångström parameter. The dynamic dependencies of dust parameters are presented as functions of optical thickness at 1020 nm, since the regressions of optical parameters with $\tau_{ext}(1020)$ were more robust than those with $\tau_{ext}(440)$ for this aerosol type.

savanna ecosystems ~85% of the biomass (largely grass) was consumed by flaming combustion while, for deforestation fires, ~50% or less of the combustion was in the flaming phase. However, differences in absorption may also be due in part to other factors such as the influence of the moisture content of the fuel, the degree of aging of the particles (Reid et al. 1999; Jacobson et al. 2001), ambient temperature, relative humidity, and fire intensity. Although high-intensity tree-crown fires are common in boreal forests, and these predominately flaming phase crown fires likely produce significant amounts of black carbon (Cofer et al. 1998), our data for boreal forest fire smoke suggest that this phase of the burning does not dominate the smoke production in the boreal zone. The relatively high ω_0 values we measure in boreal forest regions are likely due to smoldering combustion occurring over a much longer period of time relative to the comparatively short lives flaming phase of the crown fires. Radke et al. (1991) presented measurements (at 2.0–2.5-km altitude) of ω_0 as a function of time after ignition for two small North American forest fires. They showed a rapid increase in ω_0 as the fires progressed from intense burning (initial $\omega_0 < 0.7$) to predominantly smoldering combustion with the ω_0 values stabilizing at ~0.92 approximately 60 min after ignition. In the South American cerrado region, there is

TABLE 1. (*Continued*)

Urban–industrial and mixed	Mexico City (1999–2000)	Maldives (INDOEX) (1999–2000)
Number of measurements (total)	1500	700
Number of measurements (for ω_0, n, k)	300	150 (Jan–Apr)
Range of optical thickness; $\langle\tau\rangle$	$0.1 \le \tau(440) \le 1.8$; $\langle\tau(440)\rangle = 0.43$	$0.1 \le \tau(440) \le 0.7$; $\langle\tau(440)\rangle = 0.27$
Range of Ångström parameter	$1.0 \le \alpha \le 2.3$	$0.4 \le \alpha \le 2.0$
$\langle g\rangle$ (440/670/870/1020)	0.68/0.61/0.58/0.57 ± 0.07	0.74/0.67/0.64/0.63 ± 0.05
n; k	1.47 ± 0.03; 0.014 ± 0.006	1.44 ± 0.02; 0.011 ± 0.007
ω_0(440/670/870/1020)	0.90/0.88/0.85/0.83 ± 0.02	0.91/0.89/0.86/0.84 ± 0.03
r_{Vf} (μm); σ_f	0.12 + 0.04 τ(440) ± 0.02; 0.43 ± 0.03	0.18 ± 0.03; 0.46 ± 0.04
r_{Vc} (μm); σ_c	2.72 + 0.60 τ(440) ± 0.23; 0.63 ± 0.05	2.62 + 0.61 τ(440) ± 0.31; 0.76 ± 0.05
C_{Vf}(μm³/μm²)	0.12 τ(440) ± 0.03	0.12 τ(440) ± 0.03
C_{Vc}(μm³/μm²)	0.11 τ(440) ± 0.03	0.15 τ(440) ± 0.04
Biomass burning	**African savanna, Zambia (1995–2000)**	**Boreal forest, United States and Canada (1994–1998)**
Number of measurements (total)	2000	1000
Number of measurements (for ω_0, n, k)	700 (Aug–Nov)	250 (Jun–Sep)
Range of optical thickness; $\langle\tau\rangle$	$0.1 \le \tau(440) \le 1.5$; $\langle\tau(440)\rangle = 0.38$	$0.1 \le \tau(440) \le 2.0$; $\langle\tau(440)\rangle = 0.40$
Range of Ångström parameter	$1.4 \le \alpha \le 2.2$	$1.0 \le \alpha \le 2.3$
$\langle g\rangle$ (440/670/870/1020)	0.64/0.53/0.48/0.47 ± 0.06	0.69/0.61/0.55/0.53 ± 0.06
n; k	1.51 ± 0.01; 0.021 ± 0.004	1.50 ± 0.04; 0.0094 ± 0.003
ω_0(440/670/870/1020)	0.88/0.84/0.80/0.78 ± 0.015	0.94/0.935/0.92/0.91 ± 0.02
r_{Vf} (μm); σ_f	0.12 + 0.025τ(440) ± 0.01; 0.40 ± 0.01	0.15 + 0.015τ(440) ± 0.01; 0.43 ± 0.01
r_{Vc} (μm); σ_c	3.22 + 0.71τ(440) ± 0.43; 0.73 ± 0.03	3.21 + 0.2τ(440) ± 0.23; 0.81 ± 0.2
C_{Vf} (μm³/μm²)	0.12 τ(440) ± 0.04	0.01 + 0.1 τ(440) ± 0.04
C_{Vc} (μm³/μm²)	0.09 τ(440) ± 0.02	0.01 + 0.03 τ(440) ± 0.03
Desert dust and oceanic	**Cape Verde (1993–2000)**	**Lanai, HI (1995–2000)**
Number of measurements (total)	91500	800
Number of measurements (for ω_0, n, k)	300	150
Range of optical thickness; $\langle\tau\rangle$	$0.1 \le \tau(1020) \le 2.0$; $\langle\tau(1020)\rangle = 0.39$	$0.01 \le \tau(1020) \le 0.2$ $\langle\tau(1020)\rangle = 0.04$
Range of Ångström parameter	$-0.1 \le \alpha \le 0.7$	$0 \le \alpha \le 1.55$
$\langle g\rangle$ (440/670/870/1020)	0.73/0.71/0.71/0.71 ± 0.04	0.75/0.71/0.69/0.68 ± 0.04
n	1.48 ± 0.05	1.36 ± 0.01
k(440/670/870/1020)	0.0025/0.0007/0.0006/0.0006 ± 0.001	0.0015 ± 0.001
ω_0(440/670/870/1020)	0.93/0.98/0.99/0.99 ± 0.01	0.98/0.97/0.97/0.97 ± 0.03
r_{Vf} (μm); σ_f	0.12 ± 0.03; 0.49 + 0.10 τ ± 0.04	0.16 ± 0.02; 0.48 ± 0.04
r_{Vc} (μm); σ_c	1.90 ± 0.03; 0.63 − 0.10 τ ± 0.03	2.70 ± 0.04; 0.68 ± 0.04
C_{Vf} (μm³/μm²)	0.02 + 0.02 τ(1020) ± 0.03	0.40 τ(1020) ± 0.01
C_{Vc} (μm³/μm²)	0.9 τ(1020) ± 0.09	0.80 τ(1020) ± 0.02

a combination of smoke from the local burning of cerrado (savanna-like) vegetation and agricultural pasture burning in addition to the long range transport of smoke from Amazonian forest regions to the north. Thus the intermediate magnitude of ω_0 at the cerrado sites is due (Eck et al. 2001a) in part to a mixture of smoke from different source regions and also possibly from the burning of small cerrado trees that sometimes occurs associated with conversion of native cerrado ecosystems to agricultural land use. The spectral dependence and magnitude of ω_0 inferred from analysis of spectral irradiance data for a cerrado site in Brazil (Eck et al. 1998) was similar to the Amazonian forest values in Fig. 1 when transport from the north-of-forest burning smoke occurred, versus values more resembling African savanna ω_0 when smoke originated from regional cerrado burning.

Comparison of the AERONET retrievals of ω_0 for biomass-burning aerosols in South America with in situ aircraft measurements made during the Smoke, Clouds and Radiation-Brazil (SCAR-B) experiment show that AERONET values are significantly higher. For regional hazes over a region of forest in Amazonia, Reid et al. (1998) computed an average ω_0 value at 550 nm of 0.86 with a standard deviation of 0.05. This compares to an average ω_0 of 0.935 from AERONET retrieval for the same Amazonian forest region. Similarly, in situ measurement from aircraft over Brazilian cerrado site showed average $\omega_0(550) = 0.79 \pm 0.04$ for locally produced smoke and $\omega_0(550) = 0.85 \pm 0.02$ for aged smoke (Reid et al. 1998), as compared to $\omega_0(550) = 0.90 \pm 0.02$ retrieved from AERONET over Brazilian cerrado. It is noted that ω_0 determined from in situ measurement techniques are typically lower than AERONET retrieval values (see comparison for Goddard Space Flight Center (GSFC), Mexico City, and Maldives in section 3b(1). The cause for those significant differences from different measurement types (in situ versus

remote sensing) is not fully understood and should be the focus of future examination.

2) 2) PARTICLE SIZE DISTRIBUTION

The particle size distribution for all smoke from all regions investigated is dominated by the accumulation mode. Correspondingly, the following features of small particle scattering are observed: (i) high values of α (1.7 $\sim$ 2.0); (ii) the decrease of $\omega_0(\lambda)$ with increasing λ; and (iii) the pronounced decrease of the asymmetry parameter to relatively low values [from $g(440) = 0.69$ to $g(1020) = 0.52$]. At the same time, the aerosol size distributions of the smoke in these different regions also demonstrate distinct differences. The fine-mode median radius is smallest for the African savanna smoke and largest for the smoke from both forest regions (Amazonian and boreal). The larger-sized particles for smoke in forested regions may be partly a result of the greater percentage of smoldering combustion, as Reid and Hobbs (1998) measured larger particle sizes for fresh (<4 min old) smoldering smoke (0.145-μm volume median radius) than for fresh flaming-phase smoke (0.12 μm). Other factors that affect the particle size, in addition to the phase of combustion, are the characteristics of the fuel, the degree of aging of the particles, fire intensity, and ambient relative humidity and temperature. The size of the fine-mode biomass burning particles for all four regions is dynamic, exhibiting increases in size as aerosol optical depth increases. This correlation between fine-mode median particle size and τ_a is likely related to aging of the aerosol and associated changes in particle size distribution as a result of coagulation, condensation, and gas-to-particle conversion (Reid et al. 1998). Comparison of the fine-mode volume median radius of the AERONET cerrado retrievals to values measured in situ from aircraft (Differential Mobility Particle Sizes instrument) during the SCAR-B experiment (Reid et al. 1998) for a cerrado site shows similar values for both local cerrado smoke [assuming $\tau_{aer}(440) = 1.0$] and aged smoke [assuming $\tau_{aer}(440) = 2.0$].

3) 3) INDEX OF REFRACTION

The retrievals of the real part of the refractive index for biomass burning smoke range from an average of 1.47 for Amazonian forest region smoke to 1.52 for South American cerrado smoke. Yamasoe et al. (1998) also retrieved refractive indices from some of the same AERONET datasets for one of the cerrado sites but with a different methodology and found mean values ranging from 1.53 at 440 nm to 1.58 at 1020 nm. Other investigators have estimated the real part of the refractive index of biomass burning aerosols to range between $\sim$1.52 and $\sim$1.55 (Westphal and Toon 1991; Lenoble 1991; Li and Mao 1990).

b. Urban–industrial aerosol

The optical properties of urban–industrial aerosols also demonstrate significant variability, depending on the complex combination of natural and anthropogenic factors influencing aerosol formation and evolution including relative humidity, cloudiness, altitude, fuel types, emission characteristics, etc.

1) 1) SINGLE-SCATTERING ALBEDO

Haze at GSFC is almost nonabsorbing [$\omega_0(550) \sim 0.97$], while the pollution of Mexico City [$\omega_0(550) \sim 0.89$] and aerosol over the Maldives [$\omega_0(550) \sim 0.90$] absorb almost as strongly as African savanna smoke. The aerosol absorption in Creteil (a suburb of Paris) is intermediate [$\omega_0(550) \sim 0.94$–0.93] to the absorption of aerosols in GSFC and Mexico City. The retrieved low absorption values at GSFC are close to the values expected for water-soluble aerosol (Shettle and Fenn 1979; Koepke et al. 1997) with high relative humidity (Remer and Kaufman 1998; Tanré et al. 1999). However, other models give much lower ω_0 values for urban aerosol such as $\omega_0(550) \sim 0.82$ by Hess et al. (1998) and $\omega_0(550) \sim 0.84$ by Shettle and Fenn (1979) for relative humidity (RH = 90%). The AERONET retrievals for GSFC are in reasonable agreement with in situ aircraft measurements from aircraft in the SCAR-America (SCAR-A; Remer et al. 1997) and the Tropospheric Aerosol Radiative Forcing, Observational Experiment (TARFOX; Hegg et al. 1997; Russell et al. 1999; Hartley et al. 2000). The integration of aircraft in situ measurements during SCAR-A (Remer et al. 1997) show $\omega_0(450) \sim 0.98$–0.99. The TARFOX estimates (Hegg et al. 1997) of average single-scattering albedo of ambient (wet) aerosol were lower: $\omega_0(550) = 0.94$ (''mean upper limit''). However, the reanalysis of the same set of the measurements by Hartley et al. (2000) gave higher values of single-scattering albedo of hydrated aerosol [$\omega_0(550) = 0.95 \pm 0.03$]. The estimates of ω_0 by Russell et al. (1999) simulated from in situ aircraft size distribution for the values of refraction index $n = 1.4$ and $k = 0.005$ (close to our retrieval results) gave similar values [$\omega_0(550) \sim 0.95$].

The highest absorption of urban–industrial aerosol for our small sample of urban sites was observed in Mexico City [$\omega_0(550) \sim 0.90$], however it is still significantly lower than reported by many models. For example, Hess et al. (1998) give $\omega_0(550) \sim 0.84$, and Shettle and Fenn (1979) give $\omega_0(550) \sim 0.79$ for urban aerosol with RH = 80% and even lower values for RH = 50%–60%, which are typical relative humidities for Mexico City (Baumgardener et al. 2000). High aerosol absorption in Mexico City was also observed by in situ measurements (Vasilyev et al. 1995; Baumgardener et al. 2000). The estimates of single-scattering albedo from aerosol size distributions obtained by a photoelectrical counter near the ground (Vasilyev et al. 1995) gave the very low

values of $\omega_0(550) \sim 0.6$–0.8. More recent measurements of Mexico City aerosol by the nephelometer and absorption photometer (Baumgardener et al. 2000; D. Baumgardener 2001, personal communication) indicate single-scattering albedo values closer to our retrieval results $\omega_0(550) \sim 0.80$–0.88, but still lower.

The aerosol observed over the Maldives, as a part of the INDOEX experiment, shows absorption [$\omega_0(550) \sim 0.90$–0.91] that is similar to that observed for Mexico City. Such high aerosol absorption over the Maldives agrees well with other results of the INDOEX experiment conducted in the same region and for a partially overlapping time frame to our measurements (Eck et al. 2001b; R01; Satheesh et al. 1999). Several independent techniques were used during the INDOEX experiment to estimate the aerosol single-scattering albedo, ω_0, utilizing both in situ and remote sensing techniques based on measurements made from land, ships, and aircraft. Comparison of retrievals from all of these techniques with the addition of the Kaashidho Climate Observatory (KCO) AERONET (''KCO-AERONET'') retrieval (Dubovik and King 2000) was presented by Ramanathan et al. (2001). The ω_0 values estimated for 530 nm obtained by these diverse methods for the Maldives–INDOEX region ranged from ~0.86 to 0.90 for column averages. These values show good agreement, within the uncertainty levels of the AERONET and in situ retrievals (for a more detailed discussion see R01 and Eck et al. 2001b).

Unfortunately, there have not yet been any reported retrievals or measurements of ω_0 for the Paris region. Nevertheless, the existing aerosol chemical measurements (Rueallan and Cashier 2001; Liousse and Cashier 1992) near surface indicate high concentrations of black carbon in the Paris aerosol.

The observed wide variability of ω_0 for the urban locations probably can be explained by differences in fuel types, emission conditions, long-range transport and environmental and meteorological conditions. Automobile traffic around GSFC is the strongest local source of pollution, while pollution transported long distances from the Gulf of Mexico, Tennessee and Ohio valleys, etc. is also present. The mixed aerosols observed over the Maldives (INDOEX) are produced primarily as a result of anthropogenic combustion processes mainly from the use of fossil fuels (Novakov et al. 2000) with some biomass fuels and also various industrial processes. The large number of diesel vehicle and two-stroke engines is also a significant factor in aerosol formation in the Indian subcontinent (Satheesh et al. 1999). Correspondingly, the relatively strong absorption properties of the aerosols observed in the Maldives (INDOEX) is due to the presence of soot primarily from fossil fuel combustion and biomass burning, which Satheesh et al. (1999) have determined contributes ~11% to the midvisible aerosol optical depth [$\tau_{aer}(500)$]. The in situ aerosol measurements from Paris (Liousse and Cachier 1992) indicate significant presence of the atmospheric inputs from fossil fuel combustion. The intense traffic (with a larger fraction of diesel engines in Europe compared to the United States) affects the aerosol in Paris (Rueallan and Cachier 2001). Also, the transport of aerosol from Eastern Europe and the shorter distance from sources of sulfate (so that less SO_2 converts to SO_4) and/or lower emissions of SO_2 relative to the United States (due to the use of nuclear power rather than coal burning) can be important factors affecting aerosol formation in Paris. Emission controls of car and industrial pollution is more advanced in France than in Mexico and India, which may contribute to the less absorbing aerosol in Paris than in Mexico City and the Indian subcontinent.

2) 2) PARTICLE SIZE DISTRIBUTION

Comparing the particle size distribution of urban–industrial aerosol in different locations (Fig. 1, Table 1), one notes the same tendencies as those seen in ω_0 comparisons: the aerosol at GSFC is more similar to the aerosol in Creteil–Paris than to aerosols in Mexico City and the Maldives. The total volume of fine-mode particles is clearly larger than the total volume of coarse-mode particles for GSFC ($C_{Vf}/C_{Vc} \sim 3$) and Creteil ($C_{Vf}/C_{Vc} \sim 2.5$) aerosols. Nevertheless, it is noted that the retrieved optical properties of all urban–industrial aerosols sites studied are dominated by fine particle scattering. This results in $\omega_0(\lambda)$ decreasing with increasing λ, while α is quite high and the asymmetry factor g is strongly decreasing to low values with increasing λ. This domination of fine particle scattering can be explained by the fact that light in the considered spectral range (440–1020 nm) is much more efficiently scattered (cf. Bohren and Huffman 1983) by particles of fine-mode sizes ($r < 0.6$ μm) than coarse-mode particles ($r > 0.6$ μm).

Our particle size distribution retrievals agree well with various in situ aerosol measurements for the GSFC region. The in situ aircraft measurements (Hartley et al. 2000) of $dV/d\ \ln r$ show distinct bimodality (with clear domination of fine-mode volume) at different altitudes with maximums at $r_{Vf} \sim 0.15$–0.17 μm and $r_{Vc} \sim 2.5$–5 μm for $\tau_{aer}(450)$ ranging from 0.5 to 0.6. For the same optical depth levels our retrieval yields $r_{Vf} \sim 0.17$–0.18 μm and $r_{Vc} \sim 3.0$ μm. The aerosol particle size distributions retrieved from the airborne optical particle counter (Hignett et al. 1999) and nephelometer measurements (Russell et al. 1999) also show domination of fine-mode particles with $r_{Vf} \sim 0.1$–0.2 μm (after recalculating to volume distributions). The detailed comparison of the results of the ground-based size distribution retrieval (using the same AERONET measurements but a different inversion code) with aircraft in situ measurements has been performed for data of the SCAR-A experiment (Remer et al. 1997). The comparison showed good agreement of both techniques in the placement of the modes of $dV/d\ \ln r$ ($r_{Vf} \sim 0.1$–0.2 μm; $r_{Vc} \sim 1.0$–2.0

μm), with better agreement for fine-mode particles. Our retrieval shows similar values for r_{Vf}, but coarse particles have a larger size in our retrieval: $r_{Vc} \sim 3$–3.5 μm. It is important to note that the comparison of Remer et al. (1997) outlined a number of fundamental differences between remote sensing and in situ measurements, which make the comparisons of the remote sensing and in situ measurements rather difficult and uncertain.

For the Mexico City site, our observations are in qualitative agreement with available in situ measurements. Measurements (at a nearby mountain ~400 m above the city) of the mass of aerosol transported from the city basin showed significant presence (~50% of the total aerosol mass) of the large particles with the radius ~1.5–5 μm (Raga et al. 1999; Baumgardener et al. 2000). The measurement (Baumgardener et al. 2000) of the volume particle size distribution of the aerosol fine mode ($0.05 < r < 0.5$ μm) showed a maximum at $r \sim 0.15$ μm, which is in good agreement with our results [$r_{Vf} \sim 0.14$ μm at the mean $\tau_{aer}(440)$].

In order to verify the results for Maldives aerosol, a comparison of our retrieval with in situ-measured size distributions (S. Howell 2001, personal communication) vertically integrated from aircraft (~80 km from the AERONET site on Kaashidhoo) was done for one day, 7 March 1999. Some of the data corrections of the aircraft data were preliminary, however the initial comparison between the size distributions for these two very different approaches showed bimodality for both datasets with both distributions also showing very similarly sized particles for each of the modes. It is necessary to note that our data (Table 1 and Fig. 1) represent results averaged for the whole period of observations. However, as Satheesh et al. (1999) have discussed in detail, the properties of aerosol over the Maldives (during the INDOEX experiment) were rather variable. [The variations observed in AERONET retrievals are described in detail by Eck et al. (2001a).] They identified several major components to the aerosol, which contribute in varying amounts to the total loading. The fine mode aerosols observed over Maldives are produced primarily as a result of anthropogenic combustion processes mainly from the use of fossil fuels. The coarse-aerosol mode results partly from combustion processes and partly from entirely different processes and source regions. These aerosols have significant contributions from sea salt formed from the action of ocean waves and from the long distance transport of airborne soil dust from arid and semiarid regions, such as the Arabian Peninsula and the Thar Desert.

Growth of the aerosol particles

The increase in fine mode size as optical thickness increases is noticeable in our retrievals for some sites. Figure 2 illustrates the observed change of size distribution as a function of optical thickness for GSFC. It shows the increase of the median size of the fine mode with increasing optical thickness [from ~0.12 μm at $\tau_{aer}(440) = 0.04$ to ~0.21 μm at $\tau_{aer}(440) = 0.9$]. Similar growth related to optical depth magnitude can be seen for the aerosol in Creteil (Table 1). The same phenomenon was observed by both ground-based remote sensing and aircraft in situ measurements during the SCAR-A experiment in the mid-Atlantic region of the eastern United States (Remer et al. 1997). The hygroscopic growth of small particles with high humidity (Kotchenruther et al. 1999) is one of the possible mechanisms responsible for the observed increase of the median radius of the aerosol fine mode at GSFC with increasing aerosol loading. Indeed, there are a number of observations supporting this assumption. A strong correlation between aerosol optical thickness and total column water vapor content is observed at GSFC (Smirnov et al. 2000a; Holben et al. 2001). TARFOX results show that condensed water on aerosols is the main contributor to the aerosol optical thickness on the U.S. east coast (Hegg et al. 1997). The variation of the relative humidity derived from lidar measurement during the TARFOX experiment was found to be highly correlated with the effective radius derived by remote sensing techniques from aircraft measurements (Ferrare et al. 2000). In addition to hygroscopic growth, the aging processes of coagulation, condensation, and gas-to-particle conversion may also contribute to the increase in particle size (Reid et al. 1998; Jacobson 2001). Indeed, a similar but more moderate increase in fine particle size with increasing aerosol optical depth was observed at other sites (Mexico City and all biomass burning sites) where high humidity is not necessarily a primary factor. At the Maldives site this phenomenon was hidden due to the averaging performed on the retrievals for the whole measurement period (2 yr). A more detailed consideration (accounting for different aerosol sources) of the aerosol retrievals in the Maldives indicates the presence of fine-mode particle growth with optical thickness in the 1999 northeast monsoon season (Eck et al. 2001b).

It should be noted that some rather minor increase (~10%–25% of r_{Vc}) of the median radius of the coarse mode with increasing aerosol optical thickness can also be observed at urban and biomass burning sites. However, the magnitude of observed increase is comparable to the retrieval accuracy levels and there is no independent data to confirm this trend.

3) 3) INDEX OF REFRACTION

The indices of refraction [$n(\lambda)$ and $k(\lambda)$] are not independent from the $\omega_0(\lambda)$ and size distribution in our retrievals. Nevertheless, some different tendencies are obtained for the different aerosol types. Namely, for biomass burning aerosols, higher ω_0 values were correlated only with smaller values of the imaginary part of the refractive index. This kind of correlation is expected because, in the Mie formalism, $k(\lambda)$ predetermines (Bohren and Huffman 1983) the absorption of

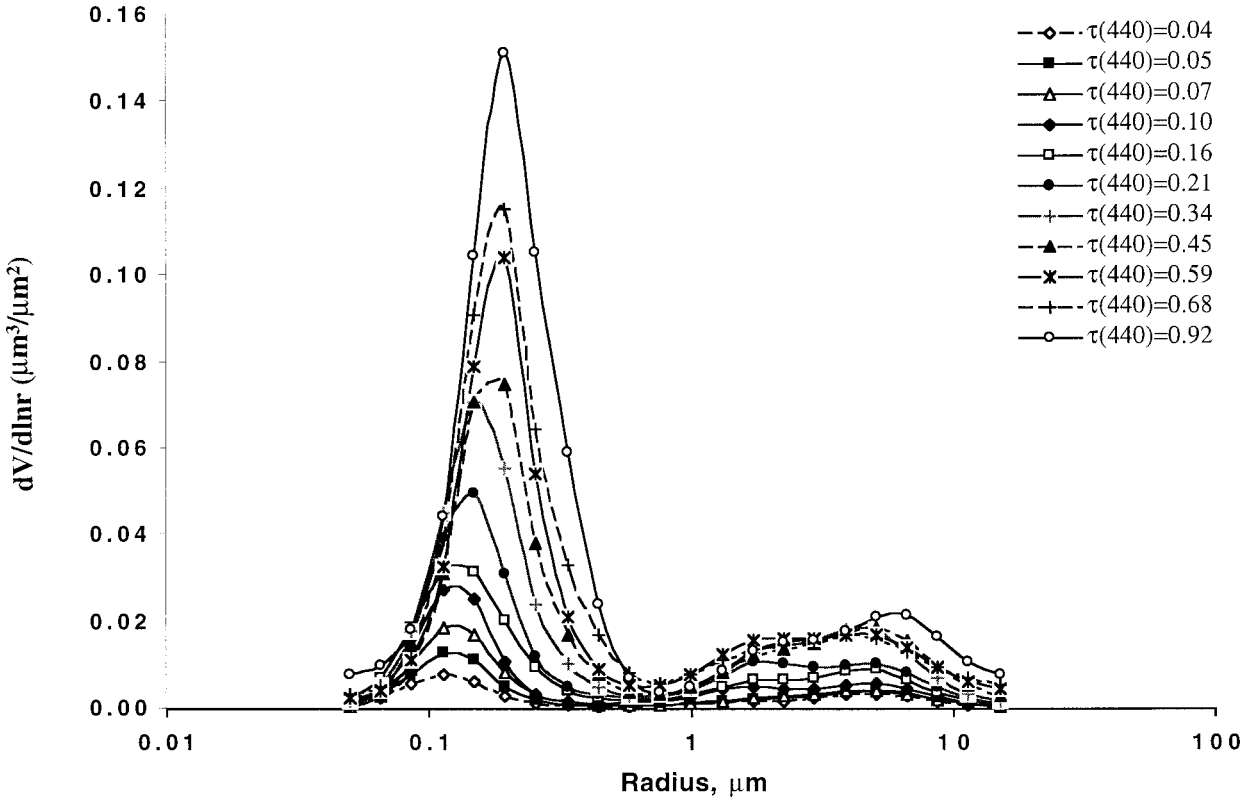

FIG. 2. The average aerosol volume size distribution retrieved at GSFC for aerosol optical thickness at 440 nm varying from 0.04 to 0.92. The aerosol size distributions were derived from the measurements of AERONET ground-based radiometers for 1993–2000 time period.

light by small particles (while the ratio of absorption to scattering + absorption also depends on particle size). For urban–industrial aerosols, higher ω_0 is somewhat correlated with lower real part of the refractive index (1.39 for GSFC, 1.40 for Creteil, 1.47 for Mexico City, and 1.44 for Maldives). This correlation is not the result of interconnections assumed by the radiative model employed. Actually, there is an opposite tendency, according electromagnetic theory (Bohren and Huffman 1983) that the total scattering increases with an increase of *n*. Therefore, this correlation likely appears due to geophysical reasons rather than interconnections assumed by the radiative model employed. The sites with lower real parts of the refractive index are possibly associated with high relative humidity and resultant aerosol hygroscopic growth (e.g., over GSFC in the summer) and the higher *n* with higher concentrations of black carbon in the atmosphere (e.g., in Mexico City and the Maldives).

The results of our refraction index retrieval agree with the results of available (unfortunately, very limited in the locations considered) independent studies. Namely, the TARFOX experiment estimates of the refractive index ranged from 1.33 to 1.45 for the real part and 0.001 to 0.008 for the imaginary part. These values were derived from a combination of aerosol in situ size distribution and remote sensing (Redemann et al. 2000) and agree well with our values for GSFC.

It should be noted that our estimates of the real part of the refractive index do not show any significant spectral dependence. However, for some cases we did observe small spectral dependence (e.g., ranging from 1.38 to 1.41 for GSFC, and from 1.42 to 1.46 for the Maldives aerosol). However, we presented only the averaged values in the Table 1 because observed spectral dependencies of *n* were within our uncertainty levels and most likely appeared due to calibration or other biases.

c. Desert dust aerosol

The domination of large particles ($r > 0.6$ μm) in desert dust aerosol (see Fig. 1 and Table 1) is the principal feature differentiating the optical properties of dust from fine-mode dominated biomass burning and urban–industrial aerosols. Therefore, in this section we first discuss the results of our size distribution retrieval followed by a discussion of the retrieved $\omega_0(\lambda)$ and index of refraction. Also, we add a discussion of the effect of particle shape, which appeared to be an issue only for our desert dust retrievals.

1) 1) PARTICLE SIZE DISTRIBUTION

The size distributions of desert dust (see Table 1 and Fig. 1) are always bimodal and dominated by large particles. Correspondingly, in contrast to biomass burning and urban–industrial aerosol, α is low (ranges from $\sim$1.2 down to -0.1) and the phase function asymmetry is relatively high at all wavelengths considered. Some differences for dust of different geographic origin are also observed. Desert dust from the western part of Africa and the Arabian Peninsula (Saudi Arabia and Cape Verde) are strongly dominated by large particles ($C_{Vc}/C_{Vf} \sim 50$) and seem to have optical properties more representative of so-called pure desert dust. The aerosol in Bahrain–Persian Gulf has a larger fine mode ($C_{Vc}/C_{Vf} \sim 10$) than observed in Saudi Arabia and in Cape Verde. This difference relates to the frequent presence in the Persian Gulf of small particles produced by industrial activity (Goloub and Arino 2000; Smirnov et al. 2002a,b). The median sizes of the fine and coarse modes ($r_{Vf} \sim 0.12$–0.15 μm and $r_{Vc} \sim 1.9$–2.54 μm) do not show any dynamics with aerosol loading and therefore have smaller values than those for biomass burning and urban–industrial aerosols for the range of high optical thickness (see Table 1). A comprehensive comparison of our results with other existing information is difficult, since the literature on dust-measured size distributions is very sparse. The in situ information is based on measurements taken mostly on ground level, while our retrieval is for the whole vertical atmospheric column. The efficiency of dust in situ sampling used in these measurements, may depend on the particle size (Fouquart et al. 1987a). The properties of the dust aerosol may also differ due to variability of sources, or distance from the source (Sokolik et al. 1998) although Carlson and Benjamin (1980) observed rather similar dust particle size in several successive Saharan dust outbreaks analyzed during the Global Atmospheric Research Program Atlantic Tropical Experiment. Our size retrievals in general agree with existing models and other independent observations. For example, in several models (Koepke et al. 1997; Tegen and Lacis 1996), the median radius of the coarse mode is about 2 μm. Measurements of Levin et al. (1980) for dust storms over the Israeli desert, and Patterson and Gillette (1977) over Texas, also show that the dust surface area distribution has a maximum around 2 μm. Dust originating from China and measured over Japan also was found to have particle radius around 2 μm (Tanaka et al. 1989). The measurements of Li-Jones and Prospero (1998), Arimoto et al. (1997) and Haywood et al. (2001; if measured dN/dr is transformed into $dV/d\ \ln r$) give size distributions with the maximum for the sizes ranging from 1.0 to 5.0 μm. At the same time, there are some disagreements with other reported data. For instance, d'Almeida and Schulz (1983) present mineral aerosol-derived particle size with maximums in a wide size range up to 100 μm and larger. Maring et al. (2000) retrieved number size distribution with number median radius $\sim$0.1 μm and less (which corresponds to volume median radius less than 1 μm). The model of Koepke et al. (1997) assumes accumulation and mineral-transported components with a maximum of the mass size distribution at $\sim$0.4–0.5 μm. Our retrievals do not show any significant presence of these components, however a minor secondary peak presents around $r = 0.5$ μm for the Cape Verde retrieval in Fig. 1.

2) 2) SINGLE-SCATTERING ALBEDO

Due to the domination of large particles, desert dust $\omega_0(\lambda)$ increases or is neutral with λ (Fig. 1 and Table 1). Our retrieved spectral single-scattering albedos suggest that dust has significantly less absorption than the 0.63–0.89 ω_0 values at 0.5 μm simulated according to several models (Shettle and Fenn 1979; WMO 1983; Koepke et al. 1997; Hess et al. 1998). This divergence is probably the result of the existing discrepancy between dust absorption reported from in situ measurements and absorption inferred from the radiation field in the atmosphere (Tanré et al. 2001, hereafter T01). The results of in situ measurements incorporated in the above models indicate the presence of significant dust absorption in the visible part of the spectrum (e.g., Patterson et al. 1977; Haywood et al. 2001). Recent satellite retrievals (Kaufman et al. 2001; T01) show low dust absorption values in the visible, results that are quite similar to our results. Some other earlier measurements and analysis (e.g., Fouquart et al. 1987b; Otterman et al. 1982; Carlson and Benjamin 1980) also support the retrieved low dust absorption in the visible to near-infrared wavelengths.

Modeling studies of the radiative properties of dust also outline some difficulties in predicting mineral dust absorption (Ackerman and Toon 1981; Claquin et al. 1998, 1999; Sokolik and Toon 1999). In fact, from the viewpoint of mineralogical composition the dust absorption is predetermined by the presence of hematite (iron oxide). Recent efforts on incorporating mineralogical composition into modeling radiative properties of dust (Claquin et al. 1998, 1999; Sokolik and Toon 1999) emphasize that the way hematite is mixed with quartz or clay is complicated and strongly impacts the resulting absorption. These mineralogical studies indicate that a lack of consideration of these mixing mechanisms is a significant limitation of the previous dust absorption computations.

It should be noted that, due to the variable presence of small particles in Bahrain, $\omega_0(\lambda)$ as well as refractive index are also very variable at this site. The refractive index and $\omega_0(\lambda)$ at Bahrain demonstrate stable values and spectral behavior consistent with those demonstrated by desert dust in other locations only when the Ångström parameter is lower than 0.6 (the details of aerosol dynamics in Bahrain are given by Smirnov et al. 2002a). For this reason, $\omega_0(\lambda)$ and refractive index, are shown

for Bahrain only for cases when the Ångström parameter is lower than 0.6. However, the particle size distribution shown for Bahrain represents all observed cases reflecting the bimodal structure of the size distribution characteristic of this location.

3) 3) INDEX OF REFRACTION

Several models suggest that the real part of the refractive index of dust is 1.53 for the visible spectral region (Shettle and Fenn 1979; WMO 1983; Koepke et al. 1997). This value is usually employed in remote sensing and allows for good consistency of radiative transfer computations with measurements (Tanré et al. 1999; T01). However, the in situ measured values reported in the literature may deviate from 1.53 (due to differences in the dust composition and probably also due to differences in the measurement techniques) with a range of about ± 0.05 or more (e.g., Patterson et al. 1977; Carlson and Benjamin 1980; Sokolik et al. 1993; Sokolik and Toon 1999). Thus, our retrieved values of 1.48–1.56 also agree in general with available dust measurements.

As discussed in section 3c(1), our retrieval shows significantly higher ω_0 values than many aerosol models suggest. Similarly, the retrieved imaginary part of the refractive index ranging from 0.0006 to 0.003 are smaller than the 0.008 value given for the visible spectrum by several models (Shettle and Fenn 1979; WMO 1983). A comparably low imaginary part of the refractive index was indicated ($k = 0.003$) by Levin et al. (1980) and ($k = 0.001$) by Otterman et al. (1982). Another feature of the retrievals is the spectral dependence of the imaginary part, where $k(\lambda)$ is 3–4 times higher at 440 than at the longer wavelengths. Such spectral dependence is not surprising for desert dust and has been reported (however for higher absolute values of k) in many studies (e.g., Patterson et al. 1977; Sokolik et al. 1993; Koepke et al. 1997; Sokolik and Toon 1999). Thus, our retrieved values of the imaginary part of the refractive index have similar spectral dependence but much lower values than were observed by in situ measurements.

4) 4) NONSPHERICITY OF DUST PARTICLES

Extensive testing of the inversion algorithm (Dubovik et al. 2000) has shown the sensitivity of AERONET retrievals to dust particle nonsphericity. According to these tests, the presence of nonspherical dust particles should result in the following retrieval artifacts: (i) high concentration of very small particles with radius less than 0.1 μm and (ii) strong spectral dependence of the real part of the refractive index [$n(\lambda)$ increases with λ]. These artifacts appear in the inversion simulation of nonspherical particles in almucantar radiances at solar zenith angle $\Theta_0 \geq 45^\circ$ (i.e., inverted scattering angles are up to double the value of the solar zenith angle) and disappear at $\Theta_0 < 20^\circ$. Features very similar to these artifacts were clearly observed in the retrievals for the observations at all desert dust sites [for $\alpha < 0.6$ and/or $\tau(1020) > 0.2$]. Figure 3 illustrates such retrieval for Bahrain for the 2 May 1999 dust event. Table 1 and Fig. 1 display only corrected retrievals of $dV/d\ln r$ and $n(\lambda)$. The applied corrections (described in section 2) allow us to retrieve a more accurate shape of $dV/d\ln r$ and value of n. However, it is important to emphasize that the Mie simulations based on the size distributions and index of refraction given in Table 1 may not reproduce accurately all of the optical properties of the dust. Namely, the appearance of artifacts in the retrievals with $\Theta_0 \geq 45^\circ$ (i.e., using measured radiances corresponding to scattering angles $\geq 90^\circ$) indicates that accurate modeling of the phase function at scattering angles $\geq 90^\circ$ needs to account for the deviations of the particle shape from spherical. Figure 4a illustrates the differences between phase functions of spheres and randomly oriented spheroids for Cape Verde desert dust [$dV/d\ln r$, $n(\lambda)$, and $k(\lambda)$ simulated according Table 1]. At the same time, the retrieval tests (Dubovik et al. 2000) and forward calculation result (Mishchenko et al. 1997) show that satisfactory values of $\omega_0(\lambda)$ as well as $g(\lambda)$ (also see Fig. 4) can be obtained by applying Mie scattering. Retrieval sensitivity tests (Dubovik et al. 2000) modeled nonspherical scattering using an approximation of the dust particle shape by randomly oriented spheroids (Mishchenko et al. 1997). This is only one of many available models of nonspherical scattering (cf. Mishchenko et al. 2000; Yang et al. 2000; Zakharova and Mischenko 2000; etc.) and it is unlikely that natural dust is represented by spheroids only. Nevertheless, the similarity of the artifacts observed in the retrievals to those observed in the sensitivity tests (Dubovik et al. 2000) used randomly oriented prolate spheroids with aspect ratio ~ 2) suggests that the chosen nonspherical model is rather adequate. Future detailed studies are necessary to clarify this issue and to incorporate nonsphericity to the AERONET retrievals.

The presence of nonsphericity in desert-dust light scattering was detected in many previous observations (cf. Nakajima et al. 1989, and detailed discussion by Mishchenko et al. 1997). However, the significance of the dust nonsphericity is not a completely clarified issue. For example, ground-based and satellite remote sensing studies (Kaufman et al. 1994; T01) did not show a significant presence of nonspherical scattering by dust (for scattering angle $\leq 120^\circ$). This possibly can be explained by the fact that a confident retrieval of nonspherical effects requires redundant spectral and, in particular, angular (in the scattering angle range from 0° to $\geq 120^\circ$) measurements. Indeed, in the studies of Kaufman et al. (1994) and T01, the retrievals of size distributions and phase functions were performed from sky radiances measured in the solar aureole (scattering angle $\leq 40^\circ$) where nonspherical effects are minimal (e.g., Fig. 4a). Also, the nonspherical scattering observed in the dust sky radiance measurements is less pronounced than it

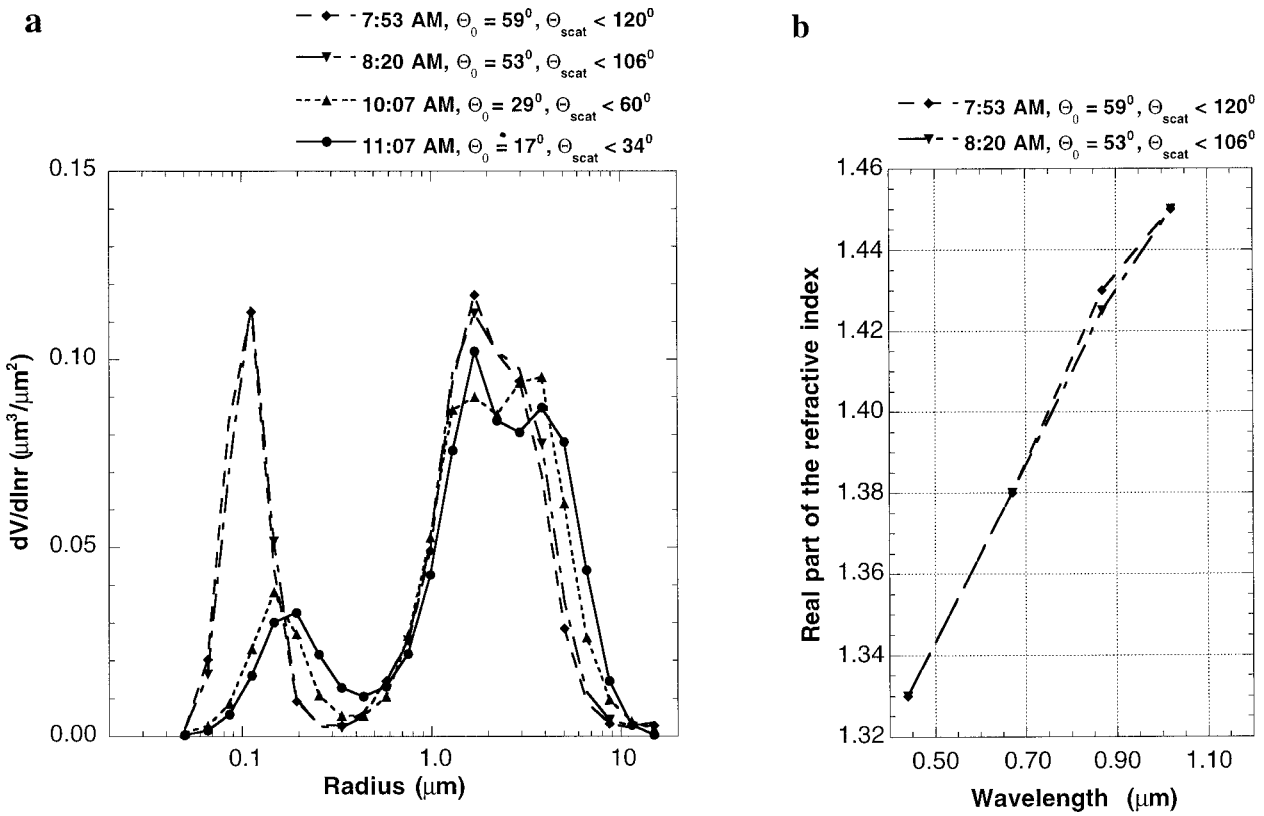

FIG. 3. Illustrations of the retrieval artifacts caused by the presence of the nonspherical particles that appear at low solar zenith angles (due to using large scattering angles in the retrieval): (a) artificially high concentrations of very small particles with radius ≤ 0.1 μm; (b) an artificial spectral dependence of the real part of the refractive index. The data presented were observed in Bahrain during a dust event on 2 May 1999, when the optical thickness of the dust was nearly constant at all wavelengths considered (within 0.02).

is in most models (probably, due to the constant presence of some fine mode particles). For example, our retrieval algorithm fit AERONET radiances measured in the almucantar with a root-mean-square of the fitting error ~15% or less. The fitting error has clear angular dependence that increases for higher scattering angles and reaches a maximum of 30%–35% at scattering angles ~100°–120° (Dubovik et al. 2000). Differences of the same magnitude were observed by T01, but were considered insignificant.

It should be noted that nonsphericity is not likely to be an issue for the fine-mode-dominated biomass burning and urban–industrial aerosols. This is because the scattering of visible and near-infrared light (we use 440–1020 nm) is not sensitive to the nonsphericity of fine mode particles [because the wave number of dominating (r_{Vf}) particles is rather small $2\pi r/\lambda < 3$]. Figure 4b illustrates that the phase functions at 440 nm of spheres and prolate spheroids with aspect ratio 2 are practically identical for Mexico City aerosol size distribution (chosen for this illustration because of pronounced presence of the coarse mode). Besides, the analysis of microscope images of biomass burning (Martins et al. 1998) and INDOEX study region particles (R01) showed that these particles were largely spherical.

d. Oceanic aerosol

Here we discuss optical properties of the aerosol observed at Lanai, Hawaii. We expect that aerosol of maritime origin dominates this aerosol, even though some influence of long-range transport of Asian dust and pollution may also be present. An important characteristic of the oceanic aerosol is the substantially lower optical thickness compared to desert dust, as well as to urban–industrial and biomass burning aerosols. The loading of oceanic aerosol usually does not exceed $\tau_{aer}(440) = 0.15$. Therefore, as shown by Dubovik et al. (2000; see section 2), the retrieval uncertainty of aerosol absorption and index of refraction is significantly higher than for other aerosols. Nevertheless, in Table 1 and Fig. 1, we complemented the retrieved size distributions (which are stable even for low aerosol loading) of oceanic aerosol by the retrieved $\omega_0(\lambda)$, n, and k values to make more complete our comparison of the optical properties of four main aerosol types. Besides, relatively small retrieval standard deviations given in Table 1 for $\omega_0(\lambda)$, n, and k indicate good stability of our results.

The aerosol observed at Lanai has a very pronounced mode of coarse particles (sea salt): $C_{Vc}/C_{Vf} \sim 2$, which is higher than for urban–industrial and biomass burning

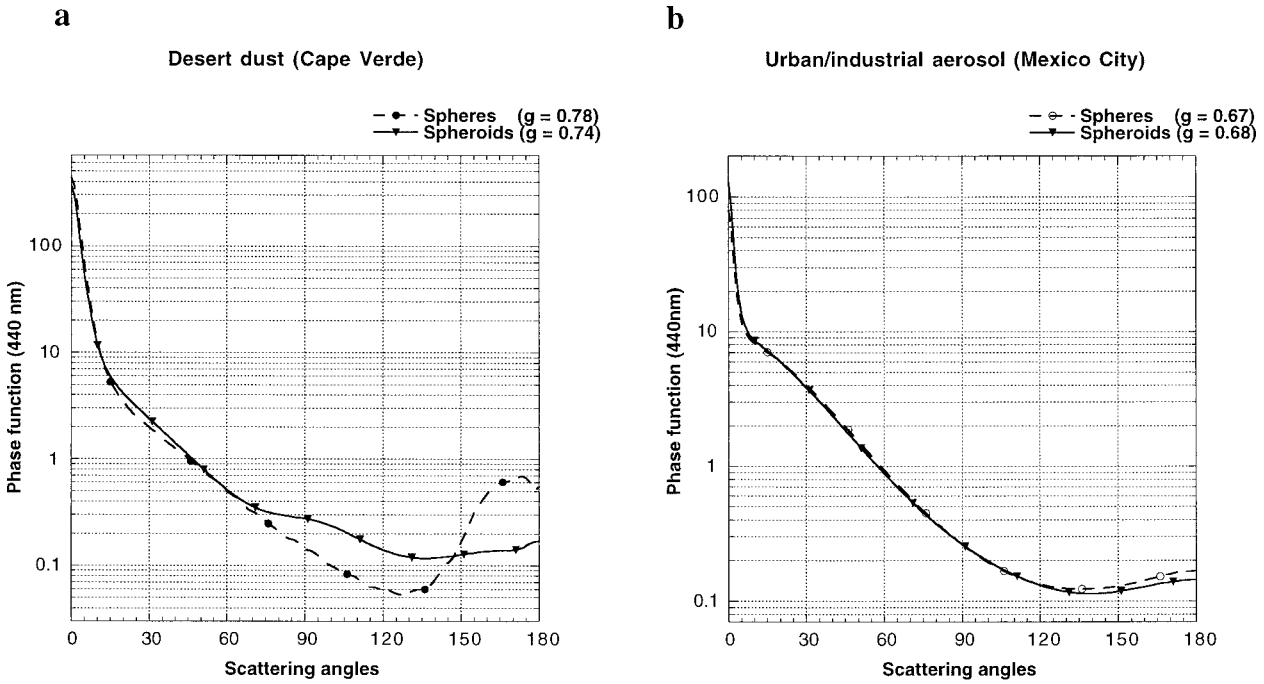

FIG. 4. (a) Illustration of the difference of the phase function of spherical particles vs spheroids for the optical models of Cape Verde dust and (b) Mexico City aerosol for an aerosol loading $\tau_{aer}(440) \sim 0.7$. The nonspherical scattering was approximated by a model of randomly oriented prolate spheroid with aspect ratio 2. The calculations were performed by the T-matrix code (e.g., see Mishchenko et al. 1997) for $(2\pi r/\lambda) \leq 20$ and by the geometric-optics-integral-equation method of Yang and Liou (1996) for larger particles.

aerosol but lower than for desert dust. Correspondingly, Lanai aerosol exhibits (see Table 1 and Fig. 1) low (for nondust aerosol) Ångström parameter and rather high asymmetry of the phase function [$g(440) = 0.75$; $g(670) = 0.71$; $g(870) = 0.69$; $g(1020) = 0.68$]. This observation of a substantial coarse-particles mode, in general, agrees with models (cf. Shettle and Fenn 1979; WMO 1983; Gathman 1983; Koepke et al. 1997; Hess et al. 1998; Tanré et al. 1999) that assume the domination of large sea-salt particles in oceanic aerosol. The low absorption ($\omega_0 \geq 0.97$) and the value of the complex refractive index ($n = 1.36$; $k = 0.0015$) agree reasonably well with the expectations for sea-salt and water-soluble particles with high relative humidity (cf. Shettle and Fenn 1979; WMO 1983; Koepke et al. 1997; Hess et al. 1998; Tanré et al. 1999).

More detailed and comprehensive analysis of the optical depth and size distributions retrieved for several oceanic AERONET sites can be found in the paper by Smirnov et al. (2002b).

4. Conclusions

This paper presents aerosol optical properties retrieved in key geographic locations as they vary with the aerosol column loading. The extensive AERONET database of several measurements per day for 2–6 yr for each site, in conjunction with advanced retrieval techniques, was used for this purpose. The data allowed the development of robust models of real undisturbed aerosols in the total atmospheric column and, for the first time, allow quantitative comparison of the average optical properties between aerosols of different types as well as within the same type of aerosol but in different geographical locations. While the reported data agree with known aerosol information in some cases (cf. Shettle and Fenn 1979; WMO 1983; Koepke et al. 1997; Hess et al. 1998), they reveal several important differences and clarify some features inherent for each type of aerosol [e.g., spectral dependence of $\omega_0(\lambda)$, partition of fine- and coarse-mode in $dV/d\ \ln r$, etc.].

For example, we found that in contrast to aerosol models found in the literature, and in qualitative agreement with recent analysis of satellite data (Kaufman et al. 2001; T01), desert dust absorption of solar radiation is very weak for wavelengths greater than 550 nm ($\omega_0 \sim 0.96$–0.99). However, dust exhibits a pronounced absorption in the blue spectral range [$\omega_0(440) \sim 0.92$–0.93].

Biomass burning optical properties are related to the vegetation type burned and relative contribution of the flaming and smoldering combustion phases. Boreal and Amazonian forest fire smoke absorbs distinctly less [$\omega_0(440) \sim 0.94$] than grassland-dominated smoke from African savanna [$\omega_0(440) \sim 0.88$] and mixed-source smoke at South American cerrado sites [$\omega_0(440) \sim 0.91$].

Absorption for urban–industrial aerosol also dem-

onstrates significant variability from almost no absorption [$\omega_0(440) \sim 0.98$] at GSFC (east coast of United States) to rather strong absorption in places known for their high level of industrial pollution: $\omega_0(440) \sim 0.90$ in Mexico City, and $\omega_0(440) \sim 0.89$ for aerosol observed over the Maldives (INDOEX; aerosol transported largely from the Indian subcontinent). Aerosol over Paris is demonstrated an intermediate level of absorption [$\omega_0(440) \sim 0.93$–0.94].

Particle nonsphericity was consistently observed in desert dust retrievals as the appearance of retrieval artifacts [high concentration of very small particles with $r < 0.1$ μm and strong spectral dependence of $n(\lambda)$] associated with the presence of nonspherical particles (Dubovik et al. 2000). The similarity of these retrieval features with ones observed in numerical tests suggests that a nonspherical-scattering model of randomly oriented spheroids is rather adequate for desert dust aerosol. However, this is only a suggestion, which requires further detailed investigations and clarification.

Acknowledgments. We thank the EOS Project Science Office for continued support. We would also like to thank the following AERONET PIs for contributing data to this study: Mexico City–Amando Leyva, Observatory of Solar Radiation, IGEF-UNAM, México D.F., 04510, MEXICO; Lanai–Dennis Clark, NOAA; Christophe Pietras and Charles McClain, NASA GSFC, SIMBIOS Project, boreal forest sites; Brian Markham, NASA GSFC. We thank Dr. Niaf Al-Abbadi, KACST Saudi Arabia; B. Chatenet from LISA CNRS Universite Paris 7 et 12, who was in charge of the Creteil instrument; and M. Santos Soares, Director of the Servico National de Meteorologiae Geophysica (SNMG), Cape Verde. We also thank the AERONET staff for the data collection, calibration and processing. Additional thanks to Michael Mishchenko, NASA GISS; and Ping Yang, NASA GSFC for providing us with the codes for modeling light scattering by nonspherical particles.

APPENDIX

Formulas Utilized for Aerosol Size Distribution Parameter Calculations

Volume median radius (mean logarithm of the radius) computed for both fine and coarse modes:

$$\ln r_V = \frac{\int_{r_{min}}^{r_{max}} \ln r \frac{dV(r)}{d\ln r}\, d\ln r}{\int_{r_{min}}^{r_{max}} \frac{dV(r)}{d\ln r}\, d\ln r}. \quad \text{(A1)}$$

Standard deviation from the volume median radius:

$$\sigma_V = \sqrt{\frac{\int_{r_{min}}^{r_{max}} (\ln r - \ln r_V)^2 \frac{dV(r)}{d\ln r}\, d\ln r}{\int_{r_{min}}^{r_{max}} \frac{dV(r)}{d\ln r}\, d\ln r}}. \quad \text{(A2)}$$

Volume concentration ($\mu m^3/\mu m^2$):

$$C_V = \int_{r_{min}}^{r_{max}} \frac{dV(r)}{d\ln r}\, d\ln r. \quad \text{(A3)}$$

REFERENCES

Ackerman, A. S., O. B. Toon, D. E. Stevens, A. J. Heymsfield, V. Ramanathan, and E. J. Welton, 2000: Reduction of tropical cloudiness by soot. *Science,* **288,** 1042–1047.

Ackerman, P., and O. B. Toon, 1981: Absorption of visible radiation in atmosphere containing mixtures of absorbing and nonabsorbing particles. *Appl. Opt.,* **20,** 3661–3668.

Ångström, A., 1929: On the atmospheric transmission of sun radiation and on dust in the air. *Geogr. Ann.,* **11,** 156–166.

Arimoto, R., B. J. Ray, N. F. Lewis, U. Tomza, and R. A. Duce, 1997: Mass-particle size distributions of atmospheric dust and the dry deposition of dust to the remote ocean. *J. Geophys. Res.,* **102,** 15 867–15 874.

Baumgardner, D., G. B. Raga, G. Kok, J. Ogren, I. Rosas, A. Baez, and T. Novakov, 2000: On the evolution of aerosol properties at a mountain site above Mexico City. *J. Geophys. Res.,* **105,** 22 243–22 253.

Bohren, C. F., and D. R. Huffman, 1983: *Absorption and Scattering of Light by Small Particles.* John Wiley and Sons, 550 pp.

Carlson, T. N., and S. G. Benjamin, 1980: Radiative heating rates of Saharan dust. *J. Atmos. Sci.,* **37,** 193–213.

Charlson, R. J., S. E. Schwartz, J. M. Hales, R. D. Cess, J. A. Coakley Jr., J. E. Hansen, and D. J. Hofmann, 1992: Climate forcing by anthropogenic aerosol. *Science,* **255,** 423–430.

Claquin, T., M. Schulz, Y. Balkanski, and O. Boucher, 1998: Uncertainties in assessing radiative forcing by mineral dust. *Tellus,* **50,** 491–505.

——, ——, and ——, 1999: Modeling the mineralogy of atmospheric dust sources. *J. Geophys. Res.,* **104,** 22 243–22 256.

Cofer, W. R., E. L. Winstead, B. J. Stocks, J. G. Goldammer, and D. R. Cahoon, 1998: Crown fire emissions of CO_2, CO, H_2, CH_4, and TNMHC from a dense jack pine boreal forest fire. *Geophys. Res. Lett.,* **25,** 3919–3922.

d'Almeida, G. A., and L. Schutz, 1983: Number, mass and volume distribution of aerosol and soils of the Sahara. *J. Climate Appl. Meteor.,* **22,** 233–243.

Dubovik, O., and M. D. King, 2000: A flexible inversion algorithm for retrieval of aerosol optical properties from sun and sky radiance measurements. *J. Geophys. Res.,* **105,** 20 673–20 696.

——, B. N. Holben, Y. J. Kaufman, M. Yamasoe, A. Smirnov, D. Tanre, and I. Slutsker, 1998: Single-scattering albedo of smoke retrieved from the sky radiance and solar transmittance measured from ground. *J. Geophys. Res.,* **103,** 31 903–31 924.

——, A. Smirnov, B. N. Holben, M. D. King, Y. J. Kaufman, T. F. Eck, and I. Slutsker, 2000: Accuracy assessment of aerosol optical properties retrieval from AERONET sun and sky radiance measurements. *J. Geophys. Res.,* **105,** 9791–9806.

Eck, T. F., B. N. Holben, I. Slutsker, and A. Setzer, 1998: Measurements of irradiance attenuation and estimation of aerosol single scattering albedo for biomass burning aerosols in Amazonia. *J. Geophys. Res.,* **103,** 31 865–31 878.

——, and Coauthors, 2001a: Characterization of the optical properties of biomass burning aerosols in Zambia during the 1997 ZIBBEE field campaign. *J. Geophys. Res.,* **106,** 3425–3448.

——, and Coauthors, 2001b: Column integrated aerosol optical properties over Maldives during NE monsoon for 1998–2000. *J. Geophys. Res.,* **106,** 28 555–28 566.

Ferrare, R., and Coauthors, 2000: Comparison of aerosol optical properties and water vapor among ground and airborne lidars and sun photometers during TARFOX. *J. Geophys. Res.,* **105,** 9917–9933.

Fouquart, Y., B. Bonnel, M. C. Roquai, R. Santer, and A. Cerf, 1987a: Observations of Saharan aerosols: Results of ECLATS field experiment. Part I: Optical thicknesses and aerosol size distributions. *J. Climate Appl. Meteor.,* **26,** 28–37.

——, ——, J. C. Brogniez, L. Buriez, L. Smith, and J. J. Morcrette, 1987b: Observations of Saharan aerosols: Results of ECLATS Field experiment. Part II: Broadband radiative characteristics of the aerosols and vertical radiative flux divergence. *J. Climate Appl. Meteor.,* **26,** 38–52.

Gathman, S. G., 1983: Optical properties of the marine aerosol as predicted by the Navy aerosol model. *Opt. Eng.,* **22,** 57–63.

Goloub, P., and O. Arino, 2000: Verification of the consistency of POLDER aerosol index over land with ATSR-2 fire product. *Geophys. Res. Lett.,* **27,** 899–902.

Hansen, J., M. Sato, and R. Ruedy, 1997: Radiative forcing and climate response. *J. Geophys. Res.,* **102,** 6831–6864.

——, ——, ——, A. Lacis, and V. Oinas, 2000: Global warming in the twenty-first century: An alternative scenario. *Proc. Natl. Acad. Sci. USA,* **97,** 9875–9880.

Hartley, W. S., P. V. Hobbs, J. L. Ross, P. B. Russell, and J. M. Livingston, 2000: Properties of aerosols aloft relevant to direct radiative forcing off the mid-Atlantic coast of the United States. *J. Geophys. Res.,* **105,** 9859–9885.

Haywood, J. M., P. N. Francis, M. D. Glew, and J. P. Taylor, 2001: Optical properties and direct radiative effect of Saharan dust: A case study of two Saharan dust outbreaks using aircraft data. *J. Geophys. Res.,* **106,** 18 417–18 430.

Hegg, D. A., J. Livingston, P. V. Hobbs, T. Novakov, and P. Russell, 1997: Chemical apportionment of aerosol column optical depth off the mid-Atlantic coast of the United States. *J. Geophys. Res.,* **102,** 25 293–25 303.

Heintzenberg, J., R. J. Charlson, A. D. Clarke, C. Liousse, V. Ramaswamy, K. P. Shine, M. Wendisch, and G. Helas, 1997: Measurements and modeling of aerosol single scattering albedo: Progress, problems and prospects. *Beitr. Phys. Atmos.,* **70,** 249–263.

Hess, M., P. Koepke, and I. Schult, 1998: Optical properties of aerosols and clouds: The software package OPAC. *Bull. Amer. Meteor. Soc.,* **79,** 831–844.

Hignett, P., J. P. Taylor, P. N. Francis, and M. D. Glew, 1999: Comparison of observed and modeled direct aerosol forcing during TARFOX. *J. Geophys. Res.,* **104,** 2279–2287.

Holben, B. N., and Coauthors, 1998: AERONET—A federated instrument network and data archive for aerosol characterization. *Remote Sens. Environ.,* **66,** 1–16.

——, and Coauthors, 2001: An emerging ground-based aerosol climatology: Aerosol optical depth from AERONET. *J. Geophys. Res.,* **106,** 9807–9826.

Houghton, J. T., L. G. Miera Filho, B. A. Callander, N. Harris, A. Kattenberg, and K. Maskell, Eds., 1996: *Climate Change 1995: The Science of Climate Change.* Intergovernmental Panel on Climate Change, Cambridge University Press, 552 pp.

Jacobson, M. Z., 2001: Strong radiative heating due to the mixing state of black carbon in atmospheric aerosols. *Nature,* **409,** 695–697.

Kahn, R., R. West, D. McDonald, B. Rheingans, and M. I. Mishchenko, 1997: Sensitivity of multiangle remote sensing observations to aerosol sphericity. *J. Geophys. Res.,* **102,** 16 861–16 870.

——, P. Banerjee, D. McDonald, and D. J. Diner, 1998: Sensitivity of multiangle imaging to aerosol optical depth and to pure-particle size distribution and composition over ocean. *J. Geophys. Res.,* **103,** 32 195–32 213.

Kaufman, Y. J., A. Gitelson, A. Karnieli, E. Ganor, R. S. Fraser, T. Nakajima, S. Mattoo, and B. N. Holben, 1994: Size distribution and phase function of aerosol particles retrieved from sky brightness measurements. *J. Geophys. Res.,* **99,** 10 341–10 356.

——, and Coauthors, 1997a: Passive remote sensing of tropospheric aerosol and atmospheric correction for the aerosol effect. *J. Geophys. Res.,* **102,** 16 815–16 830.

——, D. Tanré, L. A. Remer, E. F. Vermote, A. Chu, and B. N. Holben, 1997b: Operational remote sensing of tropospheric aerosol over land from EOS moderate resolution imaging spectroradiometer. *J. Geophys. Res.,* **102,** 17 051–17 067.

——, ——, O. Dubovik, A. Karnieli, and L. A. Remer, 2001: Absorption of sunlight by dust as inferred from satellite and ground-based remote sensing. *Geophys. Res. Lett.,* **28,** 1479–1483.

King, M. D., Y. J. Kaufman, D. Tanré, and T. Nakajima, 1999: Remote sensing of tropospheric aerosols from space: Past, present, and future. *Bull. Amer. Meteor. Soc.,* **80,** 2229–2259.

Koepke, P., M. Hess, I. Schult, and E. P. Shettle, 1997: Global aerosol data set. MPI Meteorologie Hamburg Rep. 243, 44 pp.

Kotchenruther, R., P. V. Hobbs, and D. A. Hegg, 1999: Humidification factors for atmospheric aerosols off the mid-Atlantic coast of the United States. *J. Geophys. Res.,* **104,** 2239–2251.

Krotkov, N. A., D. E. Flittner, A. J. Krueger, A. Kostinski, C. Riley, W. Rose, and O. Torres, 1999: Effect of particle nonsphericity on satellite monitoring of drifting volcanic ash clouds. *J. Quant. Spectrosc. Radiat. Transfer,* **63,** 613–630.

Lenoble, J., 1991: The particulate matter from biomass burning: A tutorial and critical review of its radiative impact. *Global Biomass Burning: Atmospheric, Climatic, and Biospheric Implications,* J. S. Levine, Ed., MIT Press, 381–386.

Levin, Z., J. H. Joseph, and Y. Mekler, 1980: Properties of Sharav (Khamsin) dust—Comparison of optical and direct sampling data. *J. Atmos. Sci.,* **37,** 882–891.

Li, J., and J. Mao, 1990: Properties of atmospheric aerosols inverted from optical remote sensing. *Atmos. Environ.,* **24A,** 2517–2522.

Li-Jones, X., and J. M. Prospero, 1998: Variations in the size distribution of non-sea-salt sulfate aerosol in the marine boundary layer at Barbados: Impact of African dust. *J. Geophys. Res.,* **103,** 16 073–16 084.

Liousse, C., and H. Cachier, 1992: Measurements of black carbon aerosols in the atmosphere of 2 different source regions—Real-time data for the Paris region and Savanna site of the Ivory Coast. *Environ. Technol.,* **13,** 959–967.

Maring, H., D. L. Savoie, M. A. Izaguirre, C. McCormick, R. Arimoto, J. M. Prospero, and C. Pilinis, 2000: Aerosol physical and optical properties and their relationship to aerosol composition in the free troposphere at Izana, Tenerife, Canary Islands, during July 1995. *J. Geophys. Res.,* **105,** 14 677–14 700.

Martins, J. V., P. Artaxo, C. Liousse, J. S. Reid, P. V. Hobbs, and Y. J. Kaufman, 1998: Effects of black carbon content, particle size, and mixing on light absorption by aerosol from biomass burning in Brazil. *J. Geophys. Res.,* **103,** 32 041–32 050.

Martonchik, J. V., D. J. Diner, R. A. Kahn, T. P. Ackerman, M. E. Verstraete, B. Pinty, and H. R. Gordon, 1998: Techniques for the retrieval of aerosol properties over land and ocean using multiangle imaging. *IEEE Trans. Geosci. Remote Sens.,* **36,** 1212–1227.

Mishchenko, M. I., J. W. Hovenier, and L. D. Travis, Eds., 2000: *Light Scattering by Nonspherical Particles.* Academic Press, 690 pp.

——, L. W. Travis, R. A. Kahn, and R. A. West, 1997: Modeling phase functions for dustlike tropospheric aerosols using a shape mixture of randomly oriented polydisperse spheroids. *J. Geophys. Res.,* **102,** 16 831–16 847.

——, I. V. Geogdzhayev, B. Cairns, W. B. Rossow, and A. A. Lacis, 1999: Aerosol retrievals over the ocean by use of channels 1 and 2 AVHRR data: Sensitivity analysis and preliminary results. *Appl. Opt.,* **38,** 7325–7341.

Nakajima, T., M. Tanaka, M. Yamano, M. Shiobara, K. Arao, and Y. Nakanishi, 1989: Aerosol optical characteristics in the yellow sand events observed in May, 1982. Part 2. Models. *J. Meteor. Soc. Japan,* **67,** 279–291.

Novakov, T., M. O. Andreae, R. Gabriel, T. W. Kirchstetter, O. L. Mayol-Bracero, and V. Ramanathan, 2000: Origin of carbonaceous aerosols over the tropical Indian Ocean: Biomass burning or fossil fuels? *Geophys. Res. Lett.,* **27,** 4061–4064.

Otterman, J., R. S. Fraser, and O. P. Bahethi, 1982: Characterization of tropospheric desert aerosols at solar wavelengths by multispectral radiometry from Landsat. *J. Geophys. Res.,* **87,** 1270–1278.

Patterson, E. M., and D. A. Gillette, 1977: Commonalities in measured size distribution for aerosol having a soil derived component. *J. Geophys. Res.,* **82,** 2074–2082.

——, ——, and B. H. Stockton, 1977: Complex index of refraction between 300 and 700 for Saharan aerosols. *J. Geophys. Res.,* **82,** 3153–3160.

Radke, L. F., and Coauthors, 1991: Particulate and trace gas emissions from large biomass fires in North America. *Global Biomass Burning: Atmospheric, Climatic, and Biopheric Implications,* J. S. Levine, Ed., MIT Press, 209–224.

Raga, G. B., D. Baumgardner, G. Kok, and I. Rosas, 1999: Some aspects of boundary layer evolution in Mexico City. *Atmos. Environ.,* **33,** 5013–5021.

Ramanathan, V., and Coauthors, 2001: The Indian Ocean Experiment: An integrated assessment of the climate forcing and effects of the Great Indo-Asian haze. *J. Geophys. Res.,* **106,** 28 371–28 398.

Redemann, J., and Coauthors, 2000: Retrieving the vertical structure of the effective aerosol complex index of refraction from a combination of aerosol in situ and remote sensing measurements during TARFOX. *J. Geophys. Res.,* **105,** 9949–9970.

Reid, J. S., and P. V. Hobbs, 1998: Physical and optical properties of young smoke from individual biomass fires in Brazil. *J. Geophys. Res.,* **103,** 32 013–32 030.

——, ——, R. J. Ferek, D. R. Blake, J. V. Martins, M. R. Dunlap, and C. Liousse, 1998: Physical, chemical, and optical properties of regional hazes dominated by smoke in Brazil. *J. Geophys. Res.,* **103,** 32 059–32 080.

——, ——, A. L. Rangno, and D. A. Hegg, 1999: Relationships between cloud droplet effective radius, liquid water content, and droplet concentration for warm clouds in Brazil embedded in biomass smoke. *J. Geophys. Res.,* **104,** 6145–6153.

Remer, L. A., and Y. J. Kaufman, 1998: Dynamic aerosol model: Urban/industrial aerosol. *J. Geophys. Res.,* **103,** 13 859–13 871.

——, S. Gasso, D. A. Hegg, Y. J. Kaufman, and B. N. Holben, 1997: Urban/industrial aerosol: Ground-based sun/sky radiometer and airborne in situ measurements. *J. Geophys. Res.,* **102,** 16 849–16 859.

——, Y. J. Kaufman, B. N. Holben, A. M. Thompson, and D. P. McNamara, 1998: Biomass burning aerosol size distribution and modeled optical properties. *J. Geophys. Res.,* **103,** 31 879–31 891.

Ruellan, S., and H. Cachier, 2001: Characterisation of fresh particulate vehicular exhausts near a Paris high flow road. *Atmos. Environ.,* **35,** 453–468.

Russell, P. B., and Coauthors, 1999: Aerosol-induced radiative flux changes off the United States mid-Atlantic coast: Comparison of values calculated from sunphotometer and in situ data with those measured by airborne pyranometer. *J. Geophys. Res.,* **104,** 2289–2307.

Satheesh, S. K., V. Ramanathan, X. Li-Jones, J. M. Lobert, I. A. Podgorny, J. M. Prospero, B. N. Holben, and N. G. Loeb, 1999: A model for natural and anthropogenic aerosols over the tropical Indian Ocean derived from Indian Ocean Experiment data. *J. Geophys. Res.,* **104,** 27 421–27 440.

Shettle, E. P., and R. W. Fenn, 1979: Models of aerosols of lower troposphere and the effect of humidity variations on their optical properties. AFCRL Tech. Rep. 79 0214, Air Force Cambridge Research Laboratory, Hanscom Air Force Base, MA, 100 pp.

Smirnov, A., B. N. Holben, O. Dubovik, N. T. O'Neill, L. A. Remer, T. F. Eck, I. Slutsker, and D. Savoie, 2000a: Measurement of atmospheric optical parameters on US Atlantic coast sites, ships and Bermuda during TARFOX. *J. Geophys. Res.,* **105,** 9887–9901.

——, ——, T. F. Eck, O. Dubovik, and I. Slutsker, 2000b: Cloud screening and quality control algorithms for the AERONET data base. *Remote Sens. Environ.,* **73,** 73 337–73 349.

——, and Coauthors, 2002a: Atmospheric aerosol optical properties in the Persian Gulf. *J. Atmos. Sci.,* **59,** 620–634.

——, ——, Y. J. Kaufman, O. Dubovik, T. F. Eck, I. Slutsker, C. Pietras, and R. N. Halthore, 2002b: Optical properties of atmospheric aerosol in maritime environments. *J. Atmos. Sci.,* **59,** 501–523.

Sokolik, I. N., and O. B. Toon, 1996: Direct radiative forcing by anthropogenic airborne mineral aerosol. *Nature,* **381,** 681–683.

——, and ——, 1999: Incorporation of mineralogical composition into models of the radiative properties of mineral aerosol from UV to IR wavelengths. *J. Geophys. Res.,* **104,** 9423–9444.

——, A. Andronove, and T. C. Johnson, 1993: Complex refractive index of atmospheric dust aerosols. *Atmos. Environ.,* **27A,** 2495–2502.

——, O. B. Toon, and R. W. Bergstrom, 1998: Modeling the radiative characteristics of airborne mineral aerosols at infrared wavelengths. *J. Geophys. Res.,* **103,** 8813–8826.

Stowe, L. L., A. M. Ignatov, and R. R. Singh, 1997: Development, validation, and potential enhancements to the second-generation operational aerosol product at the National Environmental Satellite, Data, and Information Service of the National Oceanic and Atmospheric Administration. *J. Geophys. Res.,* **102,** 16 923–16 934.

Tanaka, M., T. Nakajima, M. Shiobara, M. Yamano, and K. Arao, 1989: Aerosol optical characteristics in the yellow sand events observed in May, 1982 at Nagasaki—Part 1. Observations. *J. Meteor. Soc. Japan,* **67,** 267–278.

Tanré, D., Y. J. Kaufman, M. Herman, and S. Mattoo, 1997: Remote sensing of aerosol properties over oceans using the MODIS/EOS spectral radiances. *J. Geophys. Res.,* **102,** 16 971–16 988.

——, L. R. Remer, Y. J. Kaufman, S. Mattoo, P. V. Hobbs, J. M. Livingston, P. B. Russell, and A. Smirnov, 1999: Retrieval of aerosol optical thickness and size distribution over ocean from the MODIS airborne simulator during TARFOX. *J. Geophys. Res.,* **104,** 2261–2278.

——, and Coauthors, 2001: Climatology of dust aerosol size distribution and optical properties derived from remotely sensed data in the solar spectrum. *J. Geophys. Res.,* **106,** 18 205–18 217.

Tegen, I., and A. A. Lacis, 1996: Modeling of particle size distribution and its influence on the radiative properties of mineral dust aerosol. *J. Geophys. Res.,* **101,** 19 237–19 244.

——, ——, and I. Fung, 1996: The influence on climate forcing of mineral aerosols from disturbed soils. *Nature,* **380,** 419–422.

Torres, O., P. K. Bhartia, J. R. Herman, Z. Ahmad, and J. Gleason, 1998: Derivation of aerosol properties from satellite measurements of back scattered ultraviolet radiation: Theoretical basis. *J. Geophys. Res.,* **103,** 17 099–17 110.

Vasilyev, O. B., and Coauthors, 1995: Spectral optical properties of the polluted atmosphere of Mexico City (spring summer 1992). *J. Geophys. Res.,* **100,** 26 027–26 044.

Ward, D. E., and Coauthors, 1992: Smoke and fire characteristics for cerrado and deforestation burns in Brazil: Base-B experiment. *J. Geophys. Res.,* **97,** 14 601–14 619.

——, W. M. Hao, R. A. Susott, R. E. Babbitt, R. W. Shea, J. B. Kaufman, and C. O. Justice, 1996: Effect of fuel composition on combustion efficiency and emission factors for African savanna ecosystems. *J. Geophys. Res.,* **101,** 23 569–23 576.

Westphal, D. L., and O. B. Toon, 1991: Simulations of microphysical, radiative, and dynamical processes in a continental-scale forest fire smoke plume. *J. Geophys. Res.,* **96,** 22 379–22 400.

Whitby, K. T., 1978: The physical characteristics of sulfur aerosols. *Atmos. Environ.,* **12,** 135–159.

WMO, 1983: Radiation commission of IAMAP meeting of experts on aerosol and their climatic effects. World Meteorological Organization Rep. WCP55, 28–30.

Yamasoe, M. A., Y. J. Kaufman, O. Dubovik, L. A. Remer, B. N. Holben, and P. Artaxo, 1998: Retrieval of the real part of the refractive index of smoke particles from sun/sky measurements during SCAR-B. *J. Geophys. Res.,* **103,** 31 893–31 902.

Yang, P., and K. N. Liou, 1996: Geometric-optics-integral-equation method for light scattering by nonspherical ice crystals. *Appl. Opt.,* **35,** 6568–6584.

——, ——, M. I. Mishchenko, and B. C. Gao, 2000: Efficient finite-difference time-domain scheme for light scattering by dielectric particles: Application to aerosols. *Appl. Opt.,* **39,** 3727–3737.

Zakharova, N. T., and M. I. Mishchenko, 2000: Scattering properties of needlelike and platelike ice spheroids with moderate size parameters. *Appl. Opt.,* **39,** 5052–5057.